Pre-existing intra-basement shear zones influence growth and geometry of non-colinear normal faults, western Utsira High–Heimdal Terrace, North Sea

Edoseghe E. Osagiede[a,b,*], Atle Rotevatn[a], Rob Gawthorpe[a], Thomas B. Kristensen[a,1], Christopher A-L. Jackson[c], and Nicola Marsh[d]

[a]*Basin and Reservoir Studies Group (BRS), Department of Earth Science, University of Bergen, Allégaten 41, 5007, Bergen, Norway.*

[b]*Department of Geology, University of Benin, PMB 1154, Benin City, Nigeria.*

[c]*Basins Research Group (BRG), Department of Earth Science & Engineering, Imperial College, London, SW7 2BP, United Kingdom.*

[d]*Aker BP, Føniks, Munkegata 26, Trondheim, Norway.*

[*]*Corresponding author (e-mails: edoseghe.osagiede@uib.no, edoseghe.osagiede@uniben.edu; telephone: +47 97376763)*

Co-authors e-mails: atle.rotevatn@uib.no, rob.gawthorpe@uib.no, thomas.berg.kristensen@gmail.com, c.jackson@imperial.ac.uk, nicola.marsh@akerbp.com

Keywords: Non-colinear faults, Rift basins, Inherited structures, Stress perturbation, Utsira High

[1] *Present Address: Equinor ASA, Sandslivegen 90, 5254 Sandsli, Norway*

ABSTRACT

Pre-existing intra-basement shear zones can induce mechanical and rheological heterogeneities that may influence rifting and the overall *geometry* of rift-related normal faults. However, the extent to which physical and kinematic interaction between pre-existing shear zones and younger rift faults control the *growth* of normal faults is less-well understood. Using 3D reflection seismic data from the northern North Sea and quantitative fault analysis, we constrain the 3D relationship between pre-existing basement shear zones, and the geometry, evolution, and synrift depositional architecture of subsequent rift-related normal faults. We identify NE-SW- and N-S-striking rift faults that define a coeval Middle Jurassic – Early Cretaceous, non-colinear fault network. NE-SW-striking faults are parallel to underlying intra-basement shear zone. The faults either tip-out above or physically merge with the underlying shear zone. For faults that merges with the basement shear zone, a change from tabular to wedge-shaped geometry of the hangingwall synrift strata records a transition from non-rotational to rotational extension faulting, which we attribute to the time of rift fault's linkage with the shear zone, following downward propagation of its lower tip. N-S-striking faults are oblique to, and offset (rather than link with) intra-basement shear zones. These observations highlight the selective influence pre-existing intra-basement shear zones have on evolving rift-related normal faults.

1. INTRODUCTION

Rift basins often evolve on a template of crystalline basement that, due to complex pre-rift tectonic histories, are associated with strong heterogeneities such as mylonitic shear zones (e.g., Phillips et al. 2016). Examples of such rift basins include the North Sea rift basin (e.g., Ziegler, 1975; Fossen, 2010), the East Greenland rift system (e.g., Rotevatn et al., 2018), the Malawi rift system (e.g., Dawson et al., 2018), the Taranaki Basin, New Zealand (e.g., Collanega et al., in press), the Phitsanulok Basin, Thailand (e.g., Morley et al., 2007), and the Potiguar Basin, NE Brazil (e.g., Kirkpatrick et al., 2013). These pre-existing intra-basement shear zones not only induce lithological heterogeneity, but also thermal, mechanical and/or rheological heterogeneities at crustal and lithospheric scales that impact the style and duration of rifting, and the final rift geometry. In the North Sea for example, these shear zones are exposed onshore and are imaged in seismic reflection data offshore (e.g., Norton, 1987; Fossen, 1992; Reeve et al., 2013; Phillips et al., 2016; Fazlikhani et al., 2017; Lenhart et al., 2019). Although the recognition and description of intra-basement shear zones in the field may be relatively straightforward, seismic imaging of intra-basement shear zones in subsurface datasets (e.g., 2D and 3D seismic) can be limited by a combination of factors (Phillips et al., 2016). For example, seismic data may not image to the relatively deep depths at which crystalline basement occurs; even when the seismic record length is sufficient, decreasing seismic resolution with depth due to frequency attenuation may negatively impact our ability to image and therefore map intra-basement structure (Torvela et al., 2013). Furthermore, the density and seismic velocity contrasts between crystalline rocks may be relatively small, making it hard to define their boundaries, and thus the overall intra-basement structure (Phillips et al., 2016). As a result, the interaction between pre-existing basement structures, specifically shear zones and the overlying rift related normal faults is poorly constrained in nature.

Previous seismic- (e.g., Bartholomew et al., 1993; Morley et al., 2004; Phillips et al., 2016; Fazlikhani et al., 2017; Collanega et al., in press), field- (e.g., Maurin and Guiraud, 1993; Kirkpatrick et al., 2013; Salomon et al., 2015; Dawson et al., 2018; Muirhead and Kattenhorn, 2018; Rotevatn et al., 2018), and numerical and physical analogue-based (e.g., Faccenna et al., 1995; Corti et al., 2007; Aanyu and Koehn, 2011; Chattopadhyay and Chakra, 2013; Bonini et al., 2015; Deng et al., 2017b; Deng et al., 2018) studies demonstrate that inherited structures may influence the localization and geometry (especially the strike), and in particular the segmentation of younger rift-related normal faults. However, the extent to which intra-basement shear zones can potentially influence rift faulting *style and growth*, and consequently, the nature of accommodation within normal fault-controlled syn-rift depocentres, is still poorly understood.

In this study we utilise high-quality 3D seismic reflection and borehole data from the Utsira High and Heimdal Terrace, North Sea rift system to assess the overall influence of pre-existing intra-basement shear zones on the style and evolution of normal faulting, and overall rift development. The Utsira High is located approximately 200 km west of Stavanger, offshore Norway, and is one of the largest rift-related basement high in the North Sea, covering an approximate area of 4600 km^2 (Fig. 1a). It is bounded by the Stord Basin to the east, in the west by the South Viking Graben, and the south by the Ling Depression (Fig. 1a). The relatively shallow depth of the crystalline basement of the Utsira High results in the excellent imaging of intra-basement shear zones, and therefore provides an exceptional opportunity to investigate the inter-relationship between rift faulting and intra-basement shear zones. In detail we: (i) evaluate the 3D geometry of both intra-basement shear zones and rift-related normal faults, (ii) constrain the kinematic evolution of rift-related normal faults, and (iii) investigate the relationship between pre-existing intra-basement shear zones and rift-related faults. We show that, whereas the overall geometry and evolution of *some* rift-related normal faults are strongly influenced by underlying pre-existing basement shear zone, others are not, indicating that the influence of pre-existing basement shear zones on evolving rift faults could vary spatially over relatively short length-scales within a single rift. We also show an example of how the linkage of normal fault onto an underlying basement shear zone may result in a change in the style of rift-related fault from non-rotation to rotational, resulting in changes in the associated hangingwall synrift depositional architecture. This observation brings a new angle to the role of inherited structures, which may have been previously overlooked. Our results also have implication for understanding the palaeo-stress orientation during the Middle Jurassic – Early

Cretaceous rift phase, and emphasizes the uncertainty in using the strike of normal faults alone to infer extension direction.

INSERT FIGURE 1

2. REGIONAL TECTONIC FRAMEWORK AND STRATIGRAPHY

2.1 Regional Tectonic Framework

Following the culmination of the Caledonian orogeny in Silurian to Devonian, and the subsequent extensional collapse of the orogen in Middle to Late Devonian, protracted rifting throughout the Paleozoic and Mesozoic led to the development of a series of rift basins on the Norwegian Continental Shelf, including the North Sea rift basin (e.g., Ziegler, 1975; Glennie, 1986; Færseth et al., 1995; Nottvedt et al., 1995; Færseth, 1996). In the following, we provide an overview, with specific reference to formation and geometry of intra-basement structures that controlled later rift development.

2.1.1 Silurian to Devonian

The closure of the Iapetus Ocean in the Silurian to Devonian led to arc – continent and later continent – continent collision, giving rise to the Caledonian orogeny. Structures associated with this important tectonic event span the entire North Atlantic region (e.g., Glennie, 1986; McKerrow et al., 2000; Gee et al., 2008). Following the climax of Caledonian contraction, post-collisional (i.e. Devonian) extension initially led to reactivation of low-angle Caledonian thrusts (Mode I extension) (Fossen, 1992). This was followed by the development of mega-scale extensional shear zones (Mode II extension), and the formation of intermontane Devonian basins that are relatively well preserved onshore western Norway, but poorly constrained offshore (e.g., Steel et al., 1985; Norton et al., 1987; Dewey, 1988; Fossen, 1992, 2010; Bell et al., 2014; Fossen et al., 2016). Several of these extensional shear zones, for example the

Nordfjord-Sogn Detachment Zone (NSDZ), the Bergen Arcs (BASZ), the Hardangerfjord (HSZ), the Stavanger (SSZ), and the Kamøy (KSZ) shear zones have been mapped onshore SW Norway (e.g. Norton, 1987). Attempts to map offshore intra-basement structures in the northern North Sea (e.g. Smethurst, 2000; Phillips et al., 2016; Fazlikhani et al., 2017) have revealed a probable onshore-offshore continuity of some of the Devonian shear zones (i.e. the NSDZ, HSZ, SSZ), and revealed others, such as the Utsira Shear Zone (USZ), that appear to be restricted to the offshore (e.g. Fazlikhani et al., 2017) (Fig. 1a). These pre-Mesozoic intra-basement structural grains had a variable influence on the geometric configuration and evolution of the Mesozoic rift phases of the North Sea rift system (e.g. Johnson and Dingwall, 1981; Bartholomew et al., 1993; Færseth et al., 1995; Reeve et al., 2013; Fossen et al., 2016; Phillips et al., 2016; Fazlikhani et al., 2017).

2.1.2 Permian to Early Triassic

The first main rift phase in the northern North Sea occurred during the Permo-Triassic (Ziegler, 1975; Færseth, 1996), and is here referred to as rift phase 1 (‘RP1’). Rifting lasted between 25-37 Myr, and coincided with the break-up of Pangea (e.g., Ziegler, 1992; Ter Voorde et al., 2000). Most extensional strain was accommodated in the Horda Platform – Stord Basin and in the East Shetland Basin, where deep, wide Permo-Triassic graben and half-graben developed (Fig. 1). The dominance of N-trending Permo-Triassic basins and their bounding faults suggests an E-W principal extension axis for RP1 (e.g., Færseth, 1996; Bell et al., 2014; Fossen et al., 2016). The presence of N-trending Permian dykes, onshore western Norway also supports an E-W extension direction during RP1 (e.g. Torsvik et al., 1997; Fossen, 1998).

Some authors argue that RP1 was followed by a tectonically quiescent, ‘inter-rift’ period that continued until the Middle Jurassic (e.g. Ziegler, 1990; Bartholomew et al., 1993). During this time, these authors argue, subsidence was largely driven by thermal cooling of the lithosphere and not slip on active normal faults. However, some recent studies argue that RP1 faults (in addition to newly formed, NW-SE-striking faults) were active during the latest Triassic and Early Jurassic, suggesting there may not have been an inter-rift period or that it had a relatively shorter time span (e.g., Claringbould et al., 2016; Deng et al., 2017a).

2.1.3 Jurassic to Early Cretaceous

A second rift event occurred in the Middle Jurassic to Early Cretaceous (rift phase 2 or 'RP2') (Ziegler, 1975; Ravnås and Bondevik, 1997). Unlike RP1, most of the strain associated with RP2 accumulated in the axis of the Viking Graben (Fig. 1a). Some authors argue that strain accumulation in the Viking Graben reflected the presence of a pre-RP2 thermal dome beneath the present location of the North Sea triple junction (e.g., Ziegler, 1992; Bell et al., 2014). More specifically, this thermal dome served to heat and thus weaken the lithosphere in the vicinity of the present Viking Graben, meaning it was easier to rift here than in more marginal areas previously strained during RP1 (Bell et al., 2014). The extension direction during RP2 is debated and controversial. While some authors suggest a E-W extension, coaxial with RP1 (e.g., Badley et al., 1988; Bartholomew et al., 1993; Bell et al., 2014; Reeve et al., 2015), others propose a change from E-W during RP1 to NW-SE during RP2 (e.g., Færseth, 1996; Faerseth et al., 1997). A third model envisages E-W extension during the early part of RP2, followed by NW-SE (e.g., Doré and Gage, 1987; Doré et al., 1997), and ultimately NE-SW during the latter stages of the rift event (e.g., Davies et al., 2001).

2.2 Stratigraphy

We subdivide RP2-related stratigraphy into crystalline basement, and pre-, syn-, and post-RP2 sequences (Fig. 2). The crystalline basement is characterised by variable petrologic units, which includes granodioritic, gneissic, granitic, gabbroic, quartzitic, and phyllitic rocks (e.g., Ksienzyk et al., 2013; Riber et al., 2015; Lenhart et al., 2019). Thermochronologic dating provides Silurian – Devonian ages for the basement units (e.g., Slagstad et al., 2011; Ksienzyk et al., 2013; Lundmark et al., 2014).

INSERT FIGURE 2

Pre-RP2 stratigraphy consist of Middle Permian evaporites of the Zechstein Supergroup, and Triassic to lowermost Middle Jurassic clastics of the Hegre, Statfjord, and Dunlin groups (Halland et al., 2014). The syn-RP2 sequence, which forms the focus of our study, is uppermost Middle Jurassic to Early Cretaceous, and is divided into two main groups; (i) the Vestland Group, consisting of the Sleipner (Bajocian – Early Callovian), and Hugin (Lower Bathonian – Lower Oxfordian) formations; and (ii) the Viking Group, consisting of the Heather (uppermost Oxfordian – lowermost Tithonian), and Draupne (Kimmeridgian – Berriasian) formations (Fig. 2) (Halland et al., 2014). The highly diachronous Base Cretaceous Unconformity (BCU) marks the upper limit of syn-RP2 (e.g., Bell et al., 2014). Post-RP2 sequences therefore largely lie unconformably on syn-RP2 sequences, and comprise clastic and carbonate-dominated units that are Cretaceous to Holocene.

3. DATASET AND METHODS

Our dataset consist of a merged three-dimensional seismic reflection cube covering c. 1980 km^2 (Fig. 1b). The 3-D seismic data are of good quality, with a line spacing of 12.5 m in both the inline and crossline direction. The maximum time recorded length of the data is c. 6850 ms two-way time (TWT); the data thus image intra-basement shear zones and faults hosted in the overlying sedimentary cover. The seismic data are zero-phase, displayed in SEG reverse polarity; that is, a positive reflection coefficient or downward increase in impedance contrast corresponds to a trough (blue reflection on seismic profiles). Biostratigraphically constrained well tops from 25 wells, two of which penetrate the crystalline basement (25/6-1 and 25/7-1s;

Fig. 1b), were used to calibrate the seismic data and constrain the ages of interpreted key horizons.

To aid the interpretation of intra-basement reflectivity and the normal fault network, we extracted and used two volume-based seismic attributes; reflection intensity and variance. The reflection intensity (RI) attribute responds to the energy or average amplitude of the seismic traces (Pereira, 2009), and was used to delineate the map view geometry and distribution of intra-basement structures at different depths. We preferred to use the RI attribute over other amplitude dependent attributes because it retains the frequency content of the original seismic traces (Pereira, 2009). The variance attribute computes the waveform continuity between adjacent seismic traces (e.g., Chopra and Marfurt, 2005), and was useful for mapping subtle cover faults.

To investigate the kinematics of a selection of representative rift-related normal faults, we generated throw – length (T-x) plots (e.g., Cartwright et al., 1995; Baudon and Cartwright, 2008; Jackson et al., 2017), and calculated expansion indices (EI) (e.g., Thorsen, 1963; Cartwright et al., 1998; Osagiede et al., 2014) (for details, see Appendix). T-x plots allow us to constrain the along-strike displacement distribution on major normal faults, whereas EI plots allow us constrain the periods and timing of syn-depositional fault activity or growth faulting. Tvedt et al. (2013) demonstrated that depth converting throw values measured in two-way-time (TWT) have no impact on the patterns and shapes of throw profiles and therefore, we present throw measurements (for T-x plots) in TWT. However, we use interval velocities of 4500 m/s and 6000 m/s for Jurassic – Triassic sedimentary interval and the Caledonian basement respectively, to convert throw and thickness values from time (TWT) to depth (metres) where necessary (e.g., Christiansson et al., 2000; Rosso, 2007; Osmundsen and Ebbing, 2008; Fazlikhani et al., 2017).

4. INTRA-BASEMENT STRUCTURES

4.1 Geometry of intra-basement reflections

We first describe the overall cross-sectional and map-view geometry of intra-basement reflections. We use wellbores that penetrates Caledonian crystalline rocks to identify the top basement within the 3D seismic volume. The basement is generally characterised by very low amplitude, chaotic to semi-continuous reflections (Fig. 3). However, we locally identify several distinct intra-basement reflections. The patterns of these intra-basement reflections are highly variable in terms of amplitude strength and thickness, and the geometry of the individual reflections and reflection packages. Based on these characteristics, we recognise three main intra-basement reflection (IBR) packages (IBR1-3; Fig. 3).

IBR1 is a weakly dipping packages of high-amplitude reflections, with some of internal, individual reflection dipping more steeply, and exhibit sigmoidal geometry (Figs. 3a and c). The package varies in thickness from 1000 - 2000 ms TWT (c. 3 – 6 km) (Fig. 3a). In map-view, IBR1 broadly trends NE, and is mainly restricted to the area directly underlying the Utsira High (Fig. 4). IBR1 extends eastwards beyond our data coverage (Fig. 4).

IBR2 consist of a <1000 ms TWT- (c. < 3 km) thick, W-dipping package of semi-continuous reflections that are of lower amplitude compared to IBR1 (Fig. 3e). Individual reflections are generally sub-parallel to the outer margins of the overall reflection package (Fig. 3e). Unlike IBR1, IBR2 truncates at top Basement (Fig. 3e). IBR2 underlies the Heimdal Terrace, trends broadly E, and terminates against the NE-trending IBR1 (Fig. 4). However, in the northwestern part of the study area, IBR2 trends NNW (Fig. 4).

IBR3 is similar to IBR2, consisting of semi-continuous, relatively low-amplitude reflections (Fig. 3d). However, IBR3 is substantially thinner (□ 200 ms TWT; c. 0.5 km) than IBR2. IBR3 overlies and splays upward from the deeper IBR1, intersecting the top basement (Fig. 3d).

Unlike IBR2, where IBR3 intersects top basement, top basement is offset by up to 200 ms TWT (Fig. 3d).

INSERT FIGURE 3 & 4

4.2 Interpretation of intra-basement reflections

We interpret that the low-amplitude, chaotic seismic facies characterising much of the basement represents the seismic expression of non-mylonitic basement rocks, simply referred to here as 'crystalline basement' (Fig. 3). Our preferred interpretation of the distinct intra-basement reflections is that they represent the seismic expressions of a series of highly strained, mylonitic shear zones (Fig. 3). Our interpretation is based on the sigmoidal internal geometry of the reflections, and is consistent with interpretations suggested by previous authors for intra-basement reflectivity (e.g. 'Mylonite zones' by Reeve et al., 2013; 'Devonian Mode II extensional shear zones' by Fossen et al., 2016; 'Intra-shear zone mylonites' by Phillips et al., 2016; and 'Mylonitic shear zone' by Fazlikhani et al., 2017; Lenhart et al., 2019).

To aid the interpretation of intra-basement seismic reflections and investigate why these reflections were imaged only on some seismic lines, Wang et al. (1989) generated a 2D synthetic reflection seismogram of a 3.9 km thick mylonitic shear zone in the Whipple Mountains, southeastern California. To generate an acoustic impedance profile for the shear zone, they measured P-wave velocities parallel to three principal fabric orientation for the major lithologic units. Their results demonstrate that the P-wave velocity varies with fabric orientation, and therefore determines the acoustic impedance contrast between the non-mylonitized rocks and mylonitic shear zone. This directional variability potentially impacts how and whether intra-basement shear zones are imaged in reflection seismic data. In addition, Phillips et al. (2016) perform a 1D waveform modelling to test the geological origin of observed patterns of intra-basement reflections. The result of their modelling demonstrate that the intra-basement reflection pattern may have originated from the constructive interference of reflections from approximately 100 m-spaced layers, producing the observed high-amplitude peak and trough bundles. These two models by Wang et al. (1989) and Phillips et al. (2016) can be used to explain the observed differences in the amplitudes of the intra-basement reflections. That is, the lower amplitudes of IBR2 and IBR3 compared to IBR1 may reflect: 1) the orientation of the shear zone fabric, relative to the non-mylonitized crystalline basement (Wang et al., 1989), or 2) the lack of constructive interference of reflections from intra shear zone fabrics.

The Utsira Shear Zone, which is located within the uplifted crystalline basement that forms the Utsira High, is one of the major intra-basement shear zones, offshore SW Norway (Fig. 1a) (Fossen et al., 2016; Fazlikhani et al., 2017). The Utsira Shear Zone corresponds to IBR1 – a bundle of sigmoidal-shaped high-amplitude reflections within the basement of the Utsira High (Fig. 3a - d). In map-view, it is curved, trending broadly N in the southern Utsira High, and swinging to trend NE further north (Figs. 1a and 4). Although intra-basement structures like the Utsira Shear Zone have been previously documented (e.g., Fossen et al., 2016; Fazlikhani et al., 2017), smaller, yet still acoustically and geometrically distinct intra-basement structures such as IBR2, have not. This likely reflects that fact that previous studies used only widely-spaced, 2D-seismic profiles. We refer to the newly discovered IBR2 structure as the Heimdal Shear Zone. The Heimdal Shear Zone lies within the basement of the Heimdal Terrace. In map-view, it exhibits a branching – anastomosing pattern, terminating laterally and likely downdip against the Utsira Shear Zone (Fig. 4). Like other shear zones located onshore and offshore North Sea, we link the development of the Utsira and Heimdal shear zones with post-collisional, Devonian collapse of the Caledonian orogen (e.g., Fossen et al., 2016).

5. RIFT FAULT SYSTEMS

5.1 Fault Geometry

Detailed fault mapping aided with variance attribute analysis allows us to determine the overall geometry of the rift fault network at the Base Sleipner Formation (Middle Jurassic) stratigraphic level; this represents the base of the Middle Jurassic – Early Cretaceous rift phase in this part of the North Sea (Figs. 1b and 5). In map-view, the fault network is non-colinear with two dominant fault trends (Fig. 5): (i) approximately NE-SW-striking normal faults, and (ii) approximately N-S-striking normal faults. The distribution of the NE-SW- and N-S-striking normal faults broadly defines two domains; structural domain 1 and structural domain 2 (Fig. 5a - c).

INSERT FIGURE 5 & 6

5.1.1 Structural Domain 1

Structural domain 1 covers the northwestern Utsira High and part of the Heimdal Terrace, and is characterised by predominantly NE-SW-striking normal faults (Figs. 5a and b). Faults in domain 1 are up to 34 km long, with average of 10 km. Large (i.e. >200 ms TWT; c. 0.5 km displacement) normal faults are spaced c. 5 km, whereas smaller faults are spaced every several hundred metres. Most of the faults in this structural domain dip northwestward (Fig. 6b).

The largest fault in domain 1 is the NE-SW-striking, NW-dipping segment of the Western Utsira High Fault (Fig. 5a). This fault bounds the northwestern margin of the Utsira High and is c. 34 km long, curvilinear in plan-view, and listric in cross section (Figs. 5a and 6b). The present day throw – length (T-x) plot of the Western Utsira High Fault shows an overall double bell-shaped profile, defining a main, 28 km long SW segment (segment 1) and a 6 km NE segment (segment 2) (Fig. 7a). At Base Sleipner level, maximum throw the Western Utsira High Fault is 410 ms TWT, which occurs towards the centre of segment 1. The maximum throw on the segment 2 is c. 52 ms TWT; this again occurs near the centre of the segment (Fig. 7a).

At Top Basement structural level, the overall T-x profile closely mimics that of the Base Sleipner level (i.e. two segments are identified; Fig. 7a). Generally, however, throw values at this structural level are lower than at the structurally shallower Base Sleipner level. The maximum throw obtained for segments 1 and 2 at top Basement level are 363 ms TWT and 52 ms TWT respectively.

5.1.2 Structural Domain 2

Structural domain 2 covers the rest of the Heimdal Terrace, along the western part of the study area (Fig. 5). It is characterised by predominantly N-S-striking faults that are a few kilometres to up to 30 km long. Unlike domain 1, fault spacing and dip direction in domain 2 is very variable. Faults dip both to the west and to the east, resulting in a partly conjugate, and partly synthetic – antithetic style faulting (Figs. 6b and d). The synthetic – antithetic fault relationship results in the formation of several relatively narrow (1 – 4 km), N-trending intra-terrace horst, an example of which is the Heimdal High (Figs. 1b and 6d).

A representative major fault within domain 2 is the Heimdal Fault, which bounds the eastern side of the South Viking Graben. In terms of displacement at the Base Sleipner structural level, the Heimdal Fault is second largest structure (behind the Utsira High Border Fault, which extends beyond our study area) in our study area (Fig. 5a). The fault strikes N-S, dips to the W, and is composed of two segments (Fig. 5a). The northern segment is c. 22 km long and shows a broadly symmetrical bell-shaped displacement profile, but with a relatively steeper throw gradient towards the southern tip, presumably as a result of mechanical interaction with the adjacent southern segment (Fig. 7b). Maximum throw of ca. 580 ms TWT occurs near the centre of the northern segment (Fig. 7b). Relatively low-magnitude (<100 ms TWT), high-frequency changes in throw occur on the northern segment where it intersects (i.e. has a branchline with) smaller faults (F_X, F_Y, and F_Z; Fig. 7b).

A large, 33 km-long, E-dipping, N-S-striking normal fault, the Heimdal High Fault, bounds the eastern margin of the Heimdal High. The overall T-x profile of the Heimdal High Fault at Base Sleipner level is asymmetric (Fig. 7c). The profile also shows that the fault comprises three main segments that are, from south to north, 21 km, 4 km, and 8 km long (Fig. 7c). Individually, each segment exhibits a near symmetrical T-x profile, with the maximum throws (483 ms TWT, 343 ms TWT, and 275 ms TWT for south, central and north segments respectively) located at the centre of each segment (Fig. 7c). Whereas the T-x profile of both the northern and central segments has a more distinct central peak that of the southern segment is broadly flat-topped (Fig. 7c).

INSERT FIGURE 7

5.2 Kinematic Analysis

Expansion index (EI) extraction from both seismic and wellbore data, and the identification of intervals of syn-tectonic growth strata on seismic profiles enables us to constrain timing of activity of selected rift-related normal faults.

EI from wells that are located on the hangingwall (well 25/8-9) and footwall (well 25/8-7) of the NE-SW-striking Western Utsira High Fault reveal across fault thickening of the Sleipner (Bajocian – Bathonian), Hugin (Callovian – Oxfordian), and Heather and Draupne formations, with EI values of 3.45, 4.09, 2.11, and 1.50 respectively (Fig. 8a). These wells do not penetrate older stratigraphic units, so EI values between Base Sleipner Formation and Top Basement is based on a seismic section perpendicular to the fault, and located close to both the fault's maximum displacement centre and the well locations (Figs. 5a and 8a). The EI values for these packages are ≤ 1, suggesting that they were deposited before faulting (i. e. they are pre-rift; Fig. 8a). Furthermore, growth strata adjacent to the Western Utsira High Fault exhibits two types of stratal geometries (Fig. 8a). The first is tabular, where the Sleipner Formation increases in a block-wise fashion from the footwall to the hangingwall. The second is wedge-shaped, where Hugin–to-Draupne formations not only increase in thickness from the footwall to the hangingwall, but they also thicken towards the hangingwall.

A seismic section perpendicular to the northern segment of the N-S-striking Heimdal Fault shows no observable changes in the across fault strata thicknesses pre-Sleipner Formation (EI is c. 1) (Fig. 8b). Hence, the first growth strata corresponds to the deposition of the Sleipner Formation (Bajocian – Bathonian) (EI = 1.2; Fig. 8b). The Hugin Formation (Callovian – Oxfordian) (EI = 1.3) and Viking Group (Late Oxfordian – Berriasian) (EI = 1.56) also expand across and thus record slip on the Heimdal Fault (Fig. 8b).

Thickening of the Sleipner and Hugin formations towards the N-S-striking Fault H1 suggests this fault was also active during the Middle Jurassic (Fig. 8c). We are not able to calculate EI for this fault because the footwall stratigraphy is quite condensed, and there is no borehole in the hangingwall to directly constrain stratigraphic thicknesses. However, seismic data suggest pre-Sleipner strata do not thicken across Fault H1 (Fig. 8c).

INSERT FIGURE 8

Geometric and kinematic analysis performed on these representative faults provides insight on the evolution of the rift fault network. The NE-SW- and N-S-striking faults generally have an overall asymmetrical T-x profile, and throw values are higher at the Base Sleipner stratigraphic level than at the Top Basement, suggesting the faults most likely nucleated in the sedimentary cover, and then propagated upwards to the free surface and downwards into the Basement (Fig. 7). The lack of across-fault thickness changes below the Sleipner Formation suggest both fault sets initiated at the same time, no earlier than the Bajocian (c. 170 Ma) (Fig. 8). Combining these observations, we suggest that the majority of the faults nucleated at or near the depositional surface at the onset of RP2 in the Middle Jurassic (c. 170 Ma). Several of these faults, such as the Western Utsira High Fault, were active until the Early Cretaceous (c. 139 Ma), and were thus active for at least 31 Myrs.

6. GEOMETRIC RELATIONSHIP/INTERACTION BETWEEN INTRA-BASEMENT SHEAR ZONES AND RIFT FAULT SYSTEMS

In plan-view, there is a striking first-order relationship between the location and trend of the Utsira Shear Zone and some of the Jurassic rift-related normal faults as defined at Base Sleipner stratigraphic level (Fig. 5d). The Western Utsira High Fault and nearby smaller normal faults mimic the NE trend of the underlying Utsira Shear Zone (Fig. 5d). Conversely, N-S-striking faults like the Heimdal and Heimdal High faults are oblique to the underlying Heimdal Shear Zone (Fig. 5d).

In cross-section, we observe three main types of geometrical interaction between intra-basement shear zones and overlying rift-related normal faults: (i) merging (*sensu* Phillips et al., 2016), (ii) cross-cutting (*sensu* Phillips et al., 2016), and (iii) *kinematic* fault interactions. For the merging fault relationship, rift faults detach downwards into or on an underlying intra-basement shear zone, whereas for the cross-cutting fault relationship, rift faults displace underlying shear zones. Kinematic fault interaction here refers to a relationship where, although cover rift faults mimic the plan-view strike of underlying intra-basement shear zone, they however do not physically link with (but tip-out above) the shear zone at depth.

Merging fault relationships are observed in structural domain 1, where the Western Utsira High Fault detaches along the NW margin of the Utsira Shear Zone at depth of about 3.5 s TWT (Fig. 6a). Cross-cutting fault relationship characterise structural domain 2. For example, the Heimdal High Fault offset (by up to 600 ms TWT; c. 1.8 km) the Heimdal Shear Zone at a depth corresponding to c. 3.8 s TWT (Fig. 6b). Kinematic fault interaction is common in structural domain 1, where several of the rift faults vertically tip-out above the underlying Utsira Shear Zone without any visible hard linkage (Fig. 6a).

7. DISCUSSION

7.1 Role of pre-existing intra-basement shear zones

7.1.1 Influence on the geometry of rift-related faults.

The normal fault system on the NW Utsira High – Heimdal Terrace, which formed in response to Middle Jurassic – Early Cretaceous rifting, comprises of two fault sets; one that trends NE and another that trends N (Fig. 5). Two structural domains are recognised within this coeval non-colinear fault network. Structural domain 1 is located on the Utsira High and is dominated by NE-SW-striking faults. Structural domain 2 is located further west, on the Heimdal Terrace, and is dominated by N-S-striking faults (Fig. 5). As indicated earlier, a key observation we make here is that normal faults within both domains initiated and/or slipped contemporaneously, and are therefore related to the same Middle Jurassic – Early Cretaceous rift event.

Morley (2010) demonstrates that large-scale pre-existing weak zones (e.g., shear zones) that are oblique to the regional stress field can deflect the regional stress orientation in the immediate vicinity of the pre-existing weak zone. Similarly, Deng et al. (2017b) demonstrate that the strike of later phase rift faults locally rotate and align with the strike of underlying reactivated pre-existing basement weakness. In this study, several lines of evidence suggests that pre-existing intra-basement shear zones significantly influenced the 3D geometry of rift-related normal faults. The first is the striking correlation in the location and plan-view geometry of the NE-SW-striking faults and the underlying NE-SW-striking Utsira Shear Zone (Fig. 5d). The second is the fact that rift faults (e.g. the Western Utsira High Fault) locally detach onto the underlying Utsira shear zone, resulting in a change from a planar to a more listric fault geometry (Fig. 6a).

The influence of the Utsira Shear Zone on the geometry of the overlying rift faults (in structural domain 1) is due to the local perturbation of the Middle Jurassic – Early Cretaceous regional stress field induced by the shear zone. Similar observations of the correlation between pre-existing intra-basement shear zones and subsequent rift-related normal faults have been reported in other parts of the North Sea (e.g., Fossen et al., 2016; Phillips et al., 2016; Fazlikhani et al., 2017), and in other rift systems such as the Gulf of Suez, Egypt (e.g., Younes and McClay, 2002), NW Namibia (Salomon et al., 2015), the Taranaki Basin, New Zealand (Collanega et al., in press), and the Potiguar Basin, Brazil (Kirkpatrick et al., 2013).

In contrast to the NE-SW-striking faults, the N-S-striking faults (such as the Heimdal Fault) are oblique to the Utsira Shear Zone in plan-view, and displace the Heimdal Shear Zone; this suggests that these pre-existing intra-basement structures had little or no impact on their growth or final geometry (Figs. 5d and 6b). This underscores the fact that pre-existing basement shear zones may selectively influence the geometry and growth of normal faults in rift basins; i.e. some shear zones locally perturb the regional stress field, whereas others do not. Although several properties like shear zone orientation, dip, and mechanical strength may dictate whether they ultimately influence subsequent fault growth, our observations suggest that the thickness of the shear zone may also play a key role. For example, whereas a relatively thick (□ 3 km) intra-basement shear zones such as the Utsira Shear Zone influenced the growth and geometry of subsequent rift-related faults, thinner (□ 1 km) zones, such as the Heimdal shear zone, did not. This is in agreement with earlier suggestions by Kirkpatrick et al. (2013) that the influence of pre-existing basement shear zones on the architecture of subsequent rift faults is somewhat scale-dependent. Their conclusion is based on studies in the Potiguar Basin, NE Brazil, where remote sensing and field observations reveal that rift faults mimic the orientation of crustal-scale basement shear zones, but cross-cut meso-scale basement shear zones. Phillips et al. (2016) report similar observations offshore southern Norway, suggesting that thicker (1 – 2 km) intra-basement structures are preferentially reactivated while thinner (c. 100 m) structures are not, and thus do not influence the growth and geometry of later normal faults.

7.1.2 Influence on style of faulting and synrift depositional architecture

Combining observations from EI plot and growth strata geometries from seismic section, we recognise different stages in rift basin development. The oldest growth strata (Sleipner Formation) are tabular in the hangingwall of the Western Utsira High Fault, yet thicken in a blockwise fashion across the fault from footwall to hangingwall; this suggests that fault slip occurred in the absence of appreciable rotation of the hangingwall (Fig. 8a). This tabular depositional geometry likely represents deposition in a wide, gradually subsiding basin, similar to the 'proto-rift' strata described by Nottvedt et al. (1995). Younger growth strata (Hugin – Draupne Formations) not only thicken across the fault, but also have a wedge-shaped depositional geometry and expand towards the hangingwall; this suggests that, during the deposition of this interval, the hangingwall subsided *and* rotated (Fig. 8a). In this case, the wedge-shaped depositional geometry represents deposition in a fault-bounded half graben similar to the 'main rift stage' strata described by Nottvedt et al. (1995). The evolution of the Western Utsira High Fault is therefore characterised by a transition from an initial, non-rotational fault style to a rotational style (Fig. 9d).

Similar transitions from early non-rotational to later rotational extensional faulting has been reported in several fault blocks in the northern North Sea (e.g. the Oseberg fault block; Nottvedt et al., 1995; Ravnås and Bondevik, 1997; Løseth et al., 2009). In these studies, rotation of the hangingwall fault block is attributed to an increase in the rate of extensional faulting during the 'main rift stage'. In our study, our data suggests that rotation of the hangingwall block of Western Utsira High Fault may not only have been influenced by the rate of extension, but also by the presence of the pre-existing Utsira Shear Zone. We suggest that the onset of rotational faulting occurred when the fault propagated downwards and detached onto the shear zone at depth, leading to a more listric fault geometry. Based on the age of the tabular Sleipner Formation (c. 170 Ma) and the wedge-shaped Hugin Formation (c. 166 Ma), we estimate that the onset of fault block rotation occurred c. 4 Myr after fault initiation. For the first time, our study demonstrates that, beyond influencing the geometry (e.g. trend) of rift-related faults, intra-basement shear zones can also significantly impact on the style of faulting, stratal geometries, and nature of accommodation associated with rift faults.

INSERT FIGURE 9

7.2 Implication for Middle Jurassic – Early Cretaceous extension direction

Two main rift events in the Permo-Triassic and Middle Jurassic – Early Cretaceous (RP1 and RP2 respectively) strongly influenced the structural development of the North Sea rift system. Whereas there is a consensus among workers on an E-W extension direction during RP1 (e.g., Glennie, 1986; Badley et al., 1988; Bartholomew et al., 1993; Færseth, 1996; Torsvik et al., 1997; Fossen, 1998; Bell et al., 2014; Fossen et al., 2016; Deng et al., 2017a), the extension direction of RP2 remains the subject of debate. Several models have been proposed for the palaeo-stress orientation during RP2 in relation to RP1; these are summarized in Fig. 10.

Given that both the NE-SW- and N-S-striking rift faults nucleated contemporaneously in the Middle to Late Jurassic, they are therefore a product of the same rift phase (that is, RP2). The distribution of the NE-SW-striking faults is controlled by the local stress perturbation associated with the presence of the underlying Utsira Shear Zone (Figs. 5d and 9a - c). In general, the NE-SW-striking faults are smaller (in both length and throw) than the N-S-striking faults (Figs. 5a and 7). This implies that the N-S-striking faults accommodated most of the strain during rifting, and that these structures were therefore the most optimally oriented with respect to the regional extension direction. Based on this, we conclude that the extension direction during RP2 was oriented E-W (i.e. the same as RP1), and remained largely unchanged throughout the rift phase. This interpretation is constant extension direction model 3 shown in Fig. 10, and is in agreement with the conclusions of Bell et al. (2014) and Reeve et al. (2015) based on their studies in the Horda Platform area of the northern North Sea. Finally, our results underpin the need for detailed kinematic and geometric analysis of fault networks to (i) constrain the timing of faulting and (ii) eliminate faults whose geometry are influenced locally, before using such network to infer the palaeo-extension direction of rift systems; a conclusion that is similar to that of Collanega et al. (in press).

INSERT FIGURE 10

8. CONCLUSIONS

We have integrated 3D seismic reflection and wellbore data from the northwestern Utsira High – Heimdal Terrace, to constrain the overall influence of pre-existing intra-basement shear zones on the nature and style of faulting in rift basins. Our results are applicable to both the local study area and rift basins in general. Based on our results, we conclude that:

1. The influence of pre-existing intra-basement shear zones on the overall geometry and evolution of subsequent rift-related normal faults can vary from one structural domain to another in rift basins, depending on whether or not the basement shear zone locally perturbs the regional stress field. While some rift faults may align and even merge onto underlying basement shear zones, due to local stress perturbation induced by the latter, other rift faults trend perpendicular to an unperturbed regional stress orientation and cross-cut underlying basement shear zones. This is consistent with observations by Reeve et al. (2015) in the Maløy Slope area, and Phillips et al. (2016) in the southern North Sea.

2. Pre-existing intra-basement shear zones may have a much wider influence on rift basins than previously documented. We have shown an example of how the downward propagation

and eventual linkage of rift normal faults results in a change in the style of rift faulting (i.e., from non-rotational to rotational extension style), and consequently the nature of hangingwall accommodation and synrift depositional architecture. This brings a new angle to the role of inherited structures that may not have been previously considered.

3. The NE-SW- and N-S-striking faults defines a non-colinear rift fault network that initiated and evolved simultaneously during the Middle Jurassic – Early Cretaceous rift phase in the North Sea.

4. The development of non-colinear fault network in rift basins can be a consequence of several mechanisms; including the presence of pre-existing basement weak zones (see Reeve et al. 2015), and therefore, may not reflect multiple rift phases or change in regional extension direction. This underscores the potential misinterpretation of the palaeo-extension direction of rift basins, when such interpretation is solely based on the strike of rift faults.

5. The orientation of the maximum principal extensional stress in this area during the Middle Jurassic – Early Cretaceous rift phase was E-W, and it remained largely the same throughout the rift episode.

9. ACKNOWLEDGEMENT

This research forms part of the Syn-Rift Systems Project funded by the Research Council of Norway's PETROMAKS 2 programme (Project 255229) and industry partners Aker BP, ConocoPhillips, Faroe Petroleum, Equinor (former Statoil), Tullow Oil, and VNG Norge. We thank Aker BP for providing access to the 3D seismic reflection and wellbore dataset used for this study, and PGS for granting permission to show seismic sections. Thanks goes to Schlumberger and Eliis for providing academic licences for Petrel and Paleoscan software respectively to the University of Bergen, Norway. We thank Bjørn Nyberg for providing free access to the NetworkGT software. We also thank Thilo Wrona, Fabian Tillmans, Sebastian

Wolf, and Eric Salomon for constructive discussions and suggestions during the preparation of the manuscript.

APPENDIX

A. Fault throw-length (T-x) plotting

We measured throw values from equally spaced seismic sections (note that spacing interval was dependent on the length of fault), oriented orthogonal to the local fault strike. To obtain throw values, we calculate the difference in the two-way-time (TWT) values corresponding to the hangingwall and footwall cut-offs of specific horizons. We then plot the throw values against their location along the strike-length of the faults. We eliminate the effect of ductile drag or erosion of the footwall crest by projecting the attitude of the horizon outside of the eroded or drag zone (see Fig. X) (see also, Mansfield and Cartwright, 1996; Duffy et al., 2015).

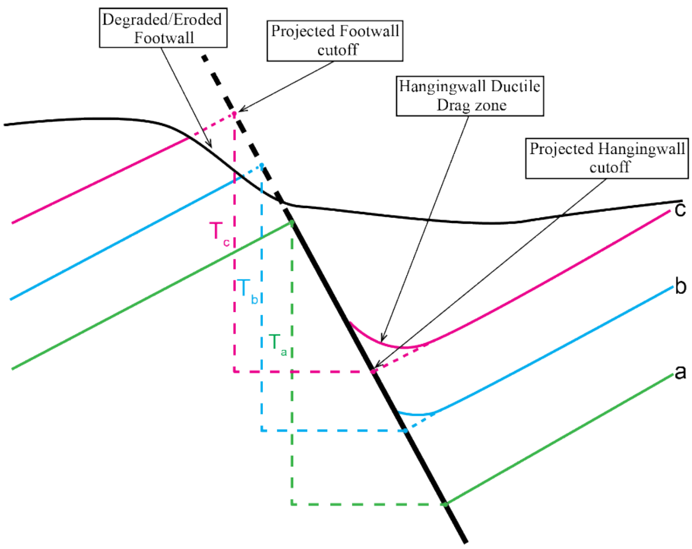

Figure X: Schematic illustration of throw measurements on faults to eliminate the effect of fault drag zone or footwall erosion. Ta, Tb, and Tc = the projected throw for horizon a, b, and c respectively.

B. Expansion Index (EI) plotting

To obtain EI values, the hangingwall thickness of fault-displaced stratigraphic unit is divided by the thickness of its footwall equivalent. The value is then plotted against the ages or depth of the units (Thorsen, 1963; see also Cartwright et al., 1998; Osagiede et al., 2014; Jackson et al., 2017). An EI of 1 means that there is no change in the hangingwall and footwall strata thickness, and therefore, suggests that activity on that particular fault post-dates deposition of the strata/unit. An EI > 1 corresponds to a thicker hangingwall strata compared to the footwall, suggesting syn-depositional fault activity (e.g., Thorsen, 1963; Cartwright et al., 1998; Osagiede et al., 2014; Jackson et al., 2017). It should be noted that, a main requirement and/or limitation of this technique is that both the hangingwall and footwall stratigraphy should be preserved and have seismically resolvable thicknesses, but this may not always be the case. For example, where little accommodation space is created; like in the case of an evolving structural high, the syn-rift strata typically have thicknesses that are below seismic resolution. Consequently, for a major rift fault whose strata thicknesses could not be resolved directly from seismic, we measured the thicknesses from wellbores that penetrates both the hangingwall and footwall of the fault, and use these measurements to generate EI plot (after Reeve et al., 2015).

REFERENCES

Aanyu, K., Koehn, D., 2011. Influence of pre-existing fabrics on fault kinematics and rift geometry of interacting segments: analogue models based on the Albertine Rift (Uganda), Western Branch-East African Rift System. Journal of African Earth Sciences 59, 168-184.

Badley, M., Price, J., Dahl, C.R., Agdestein, T., 1988. The structural evolution of the northern Viking Graben and its bearing upon extensional modes of basin formation. Journal of the Geological Society 145, 455-472.

Bartholomew, I., Peters, J., Powell, C., 1993. Regional structural evolution of the North Sea: oblique slip and the reactivation of basement lineaments, Geological Society, London, Petroleum Geology Conference series. Geological Society of London, pp. 1109-1122.

Baudon, C., Cartwright, J.A., 2008. 3D seismic characterisation of an array of blind normal faults in the Levant Basin, Eastern Mediterranean. Journal of Structural Geology 30, 746-760.

Bell, R.E., Jackson, C.A.L., Whipp, P.S., Clements, B., 2014. Strain migration during multiphase extension: observations from the northern North Sea. Tectonics 33, 1936-1963.

Bonini, L., Basili, R., Toscani, G., Burrato, P., Seno, S., Valensise, G., 2015. The role of pre-existing discontinuities in the development of extensional faults: an analog modeling perspective. Journal of Structural Geology 74, 145-158.

Cartwright, J., Bouroullec, R., James, D., Johnson, H., 1998. Polycyclic motion history of some Gulf Coast growth faults from high-resolution displacement analysis. Geology 26, 819-822.

Cartwright, J.A., Trudgill, B.D., Mansfield, C.S., 1995. Fault growth by segment linkage: an explanation for scatter in maximum displacement and trace length data from the Canyonlands Grabens of SE Utah. Journal of Structural Geology 17, 1319-1326.

Chattopadhyay, A., Chakra, M., 2013. Influence of pre-existing pervasive fabrics on fault patterns during orthogonal and oblique rifting: an experimental approach. Marine and Petroleum Geology 39, 74-91.

Chopra, S., Marfurt, K.J., 2005. Seismic attributes—A historical perspective. Geophysics 70, 3SO-28SO.

Christiansson, P., Faleide, J., Berge, A., 2000. Crustal structure in the northern North Sea: an integrated geophysical study. Geological Society, London, Special Publications 167, 15-40.

Claringbould, J., Bell, R., Jackson, C., Gawthorpe, R., Odinsen, T., 2016. Diachronous fault array growth within continental rift basins: Quantitative analyses from the East Shetland Basin, northern North Sea, EGU General Assembly Conference Abstracts.

Collanega, L., Jackson, C.A.L., Bell, R.E., Coleman, A.J., Lenhart, A., Breda, A., in press. Normal fault growth influenced by basement fabrics: the importance of preferential nucleation from pre-existing structures. Basin Research.

Corti, G., van Wijk, J., Cloetingh, S., Morley, C.K., 2007. Tectonic inheritance and continental rift architecture: Numerical and analogue models of the East African Rift system. Tectonics 26, 1-13.

Davies, R., Turner, J., Underhill, J., 2001. Sequential dip-slip fault movement during rifting: a new model for the evolution of the Jurassic trilete North Sea rift system. Petroleum Geoscience 7, 371-388.

Dawson, S.M., Laó-Dávila, D.A., Atekwana, E.A., Abdelsalam, M.G., 2018. The influence of the Precambrian Mughese Shear Zone structures on strain accommodation in the northern Malawi Rift. Tectonophysics 722, 53-68.

Deng, C., Fossen, H., Gawthorpe, R.L., Rotevatn, A., Jackson, C.A., FazliKhani, H., 2017a. Influence of fault reactivation during multiphase rifting: the Oseberg area, Northern North Sea rift. Marine and Petroleum Geology 86, 1252-1272.

Deng, C., Gawthorpe, R.L., Finch, E., Fossen, H., 2017b. Influence of a pre-existing basement weakness on normal fault growth during oblique extension: Insights from discrete element modeling. Journal of Structural Geology 105, 44-61.

Deng, C., Gawthorpe, R.L., Fossen, H., Finch, E., 2018. How Does the Orientation of a Preexisting Basement Weakness Influence Fault Development During Renewed Rifting? Insights From Three-Dimensional Discrete Element Modeling. Tectonics 37, 2221-2242.

Dewey, J.F., 1988. Extensional collapse of orogens. Tectonics 7, 1123-1139.

Doré, A., Gage, M., 1987. Crustal alignments and sedimentary domains in the evolution of the North Sea, North-east Atlantic Margin and Barents Shelf, Petroleum geology of north west Europe. Graham and Trotman London, pp. 1131-1148.

Doré, A., Lundin, E., Fichler, C., Olesen, O., 1997. Patterns of basement structure and reactivation along the NE Atlantic margin. Journal of the Geological Society 154, 85-92.

Duffy, O.B., Bell, R.E., Jackson, C.A.L., Gawthorpe, R.L., Whipp, P.S., 2015. Fault growth and interactions in a multiphase rift fault network: Horda Platform, Norwegian North Sea. Journal of Structural Geology 80, 99-119.

Faccenna, C., Nalpas, T., Brun, J.-P., Davy, P., Bosi, V., 1995. The influence of pre-existing thrust faults on normal fault geometry in nature and in experiments. Journal of Structural Geology 17, 1139-1149.

Faerseth, R., Knudsen, B., Liljedahl, T., Midbue, P., Søderstrøm, B., 1997. Oblique rifting and sequential faulting in the Jurassic development of the northern North Sea. Journal of Structural Geology 19, 1285-1302.

Fazlikhani, H., Fossen, H., Gawthorpe, R.L., Faleide, J., Bell, R.E., 2017. Basement structure and its influence on the structural configuration of the northern North Sea.

Fossen, H., 1992. The role of extensional tectonics in the Caledonides of south Norway. Journal of structural geology 14, 1033-1046.

Fossen, H., 1998. Advances in understanding the post-Caledonian structural evolution of the Bergen area, West Norway. Norsk Geologisk Tidsskrift 78, 33-46.

Fossen, H., 2010. Extensional tectonics in the North Atlantic Caledonides: a regional view. Geological Society, London, Special Publications 335, 767-793.

Fossen, H., Khani, H.F., Faleide, J.I., Ksienzyk, A.K., Dunlap, W.J., 2016. Post-Caledonian extension in the West Norway–northern North Sea region: the role of structural inheritance. Geological Society, London, Special Publications 439, SP439. 436.

Færseth, R., 1996. Interaction of Permo-Triassic and Jurassic extensional fault-blocks during the development of the northern North Sea. Journal of the Geological Society 153, 931-944.

Færseth, R., Gabrielsen, R., Hurich, C.A., 1995. Influence of basement in structuring of the North Sea basin, offshore southwest Norway. Norsk Geologisk Tidsskrift 75, 105-119.

Gee, D.G., Fossen, H., Henriksen, N., Higgins, A.K., 2008. From the early Paleozoic platforms of Baltica and Laurentia to the Caledonide Orogen of Scandinavia and Greenland. Episodes 31, 44-51.

Giba, M., Walsh, J., Nicol, A., 2012. Segmentation and growth of an obliquely reactivated normal fault. Journal of Structural Geology 39, 253-267.

Glennie, K.W., 1986. The structural framework and the pre-Permian history of the North Sea area, in: GLENNIE, K.W. (Ed.), Introduction to the Petroleum Geology of the North Sea, 2nd ed. Blackwell Scientific Publications, London, pp. 25-62.

Halland, E.K., Gjeldvik, I.T., Johansen, W.T., Magnus, C., Meling, M.I., Pedersen, S., Riis, F., Solbakk, T., Tappel, I.M., 2014. The Norwegian North Sea, CO_2 Storage Atlas: Norwegain Continental Shelf. Norwegian Petroleum Directorate, pp. 30-73.

Jackson, C.A.-L., Bell, R.E., Rotevatn, A., Tvedt, A.B., 2017. Techniques to determine the kinematics of synsedimentary normal faults and implications for fault growth models. Geological Society, London, Special Publications 439, SP439. 422.

Jackson, C.A.-L., Larsen, E., Hanslien, S., Tjemsland, A.-E., 2011. Controls on synrift turbidite deposition on the hanging wall of the South Viking Graben, North Sea rift system, offshore Norway. AAPG bulletin 95, 1557-1587.

Jardin, A., Roure, F., Nikolla, L., 2011. Subsalt depth seismic imaging and structural interpretation in Dumre area, Albania. Oil & Gas Science and Technology–Revue d'IFP Energies nouvelles 66, 911-929.

Johnson, R., Dingwall, R., 1981. The Caledonides: their influence on the stratigraphy of the northwest European continental shelf. Petroleum Geology of the Continental Shelf of North-West Europe. Heyden, London 8597.

Kirkpatrick, J., Bezerra, F., Shipton, Z., Do Nascimento, A., Pytharouli, S., Lunn, R., Soden, A., 2013. Scale-dependent influence of pre-existing basement shear zones on rift faulting: a case study from NE Brazil. Journal of the Geological Society 170, 237-247.

Ksienzyk, A.K., Jacobs, J., Fossen, H., Dunkl, I., Kosler, J., 2013. The basement of the Utsira High: U/Pb, (U-Th)/He and fission track thermochronology, in: Nakrem, H.A., Haukdal, G.K. (Eds.), Vinterkonferansen. Norsk Geologisk Forening (NGF), Oslo, p. 75.

Lenhart, A., Jackson, C.A.-L., Bell, R.E., Duffy, O.B., Gawthorpe, R.L., Fossen, H., 2019. Structural architecture and composition of crystalline basement offshore west Norway. Lithosphere, 1-21.

Lundmark, A., Sæther, T., Sørlie, R., 2014. Ordovician to Silurian magmatism on the Utsira High, North Sea: implications for correlations between the onshore and offshore Caledonides. Geological Society, London, Special Publications 390, 513-523.

Løseth, T.M., Ryseth, A.E., Young, M., 2009. Sedimentology and sequence stratigraphy of the middle Jurassic Tarbert Formation, Oseberg South area (northern North Sea). Basin Research 21, 597-619.

Mansfield, C., Cartwright, J., 1996. High resolution fault displacement mapping from three-dimensional seismic data: evidence for dip linkage during fault growth. Journal of Structural Geology 18, 249-263.

Maurin, J.-C., Guiraud, R., 1993. Basement control in the development of the Early Cretaceous West and Central African rift system. Tectonophysics 228, 81-95.

McKerrow, W., Mac Niocaill, C., Dewey, J., 2000. The Caledonian orogeny redefined. Journal of the Geological Society 157, 1149-1154.

Morley, C., 2010. Stress re-orientation along zones of weak fabrics in rifts: An explanation for pure extension in 'oblique'rift segments? Earth and Planetary Science Letters 297, 667-673.

Morley, C., Gabdi, S., Seusutthiya, K., 2007. Fault superimposition and linkage resulting from stress changes during rifting: Examples from 3D seismic data, Phitsanulok Basin, Thailand. Journal of Structural Geology 29, 646-663.

Morley, C., Haranya, C., Phoosongsee, W., Pongwapee, S., Kornsawan, A., Wonganan, N., 2004. Activation of rift oblique and rift parallel pre-existing fabrics during extension and their effect on deformation style: examples from the rifts of Thailand. Journal of Structural Geology 26, 1803-1829.

Muirhead, J., Kattenhorn, S., 2018. Activation of preexisting transverse structures in an evolving magmatic rift in East Africa. Journal of Structural Geology 106, 1-18.

Norton, M.G., 1987. The Nordfjord-Sogn Detachment, W. Norway. Norsk Geologisk Tidsskrift 67, 93-106.

Norton, M.G., McClay, K.R., Way, N.A., 1987. Tectonic evolution of Devonian basins in northern Scotland and southern Norway. Norsk Geologisk Tidsskrift 67, 323.

Nottvedt, A., Gabrielsen, R., Steel, R., 1995. Tectonostratigraphy and sedimentary architecture of rift basins, with reference to the northern North Sea. Marine and Petroleum Geology 12, 881-901.

Osagiede, E.E., Duffy, O.B., Jackson, C.A.-L., Wrona, T., 2014. Quantifying the growth history of seismically imaged normal faults. Journal of Structural Geology 66, 382-399.

Osmundsen, P., Ebbing, J., 2008. Styles of extension offshore mid-Norway and implications for mechanisms of crustal thinning at passive margins. Tectonics 27, 1-25.

Pereira, L.A.G.R., 2009. Seismic Attributes in Hydrocarbon Reservoirs Characterization. University of Aveiro, p. 165.

Phillips, T.B., Jackson, C.A.L., Bell, R.E., Duffy, O.B., Fossen, H., 2016. Reactivation of intrabasement structures during rifting: A case study from offshore southern Norway. Journal of Structural Geology 91, 54-73.

Ravnås, R., Bondevik, K., 1997. Architecture and controls on Bathonian–Kimmeridgian shallow-marine synrift wedges of the Oseberg–Brage area, northern North Sea. Basin Research 9, 197-226.

Reeve, M.T., Bell, R.E., Duffy, O.B., Jackson, C.A.L., Sansom, E., 2015. The growth of non-colinear normal fault systems; What can we learn from 3D seismic reflection data? Journal of Structural Geology 70, 141-155.

Reeve, M.T., Bell, R.E., Jackson, C.A.-L., 2013. Origin and significance of intra-basement seismic reflections offshore western Norway. Journal of the Geological Society 171, 1-4.

Riber, L., Dypvik, H., Senile, R., 2015. Altered basement rocks on the Utsira High and its surroundings, Norwegian North Sea. Norwegian Journal of Geology 95, 57-89.

Rosso, A., 2007. Deep crustal geometry: An integrated geophysical study of an exhumed Eclogite terrain, Bergen area, Southwest Norway. University of Wyoming, p. 133.

Rotevatn, A., Kristensen, T., Ksienzyk, A., Wemmer, K., Henstra, G., Midtkandal, I., Grundvåg, S.A., Andresen, A., 2018. Structural inheritance and rapid rift-length establishment in a multiphase rift: the East Greenland rift system and its Caledonian orogenic ancestry. Tectonics 37, 1858-1875.

Salomon, E., Koehn, D., Passchier, C., 2015. Brittle reactivation of ductile shear zones in NW Namibia in relation to South Atlantic rifting. Tectonics 34, 70-85.

Slagstad, T., Davidsen, B., Daly, J.S., 2011. Age and composition of crystalline basement rocks on the Norwegian continental margin: offshore extension and continuity of the Caledonian–Appalachian orogenic belt. Journal of the Geological Society 168, 1167-1185.

Smethurst, M.A., 2000. Land–offshore tectonic links in western Norway and the northern North Sea. Journal of the Geological Society 157, 769-781.

Steel, R., Siedlecka, A., Roberts, D., 1985. The Old Red Sandstone basins of Norway and their deformation: a review. The Caledonide Orogen—Scandinavia and Related Areas. Wiley, Chichester 293, 315.

Ter Voorde, M., Færseth, R., Gabrielsen, R., Cloetingh, S., 2000. Repeated lithosphere extension in the northern Viking Graben: a coupled or a decoupled rheology? Geological Society, London, Special Publications 167, 59-81.

Thorsen, C.E., 1963. Age of growth faulting in southeast Louisiana.

Torsvik, T.H., Andersen, T.B., Eide, E.A., Walderhaug, H.J., 1997. The age and tectonic significance of dolerite dykes in western Norway. Journal of the Geological Society 154, 961-973.

Torvela, T., Moreau, J., Butler, R.W., Korja, A., Heikkinen, P., 2013. The mode of deformation in the orogenic mid-crust revealed by seismic attribute analysis. Geochemistry, Geophysics, Geosystems 14, 1069-1086.

Tvedt, A.B., Rotevatn, A., Jackson, C.A.-L., Fossen, H., Gawthorpe, R.L., 2013. Growth of normal faults in multilayer sequences: A 3D seismic case study from the Egersund Basin, Norwegian North Sea. Journal of Structural Geology 55, 1-20.

Wang, C.-Y., Okaya, D.A., Ruppert, C., Davis, G.A., Guo, T.-S., Zhong, Z., Wenk, H.-R., 1989. Seismic reflectivity of the Whipple Mountain shear zone in southern California. Journal of Geophysical Research: Solid Earth 94, 2989-3005.

Younes, A.I., McClay, K., 2002. Development of accommodation zones in the Gulf of Suez-Red Sea rift, Egypt. AAPG bulletin 86, 1003-1026.

Ziegler, P., 1975. Geologic evolution of North Sea and its tectonic framework. AAPG Bulletin 59, 1073-1097.

Ziegler, P., 1990. Tectonic and palaeogeographic development of the North Sea rift system, Tectonic evolution of the North Sea rifts. Oxford Science Publications Oxford, pp. 1-36.

Ziegler, P., 1992. North Sea rift system. In: P.A. Ziegler (Eds.), Geodynamics of Rifting, Volume I. Case History Studies on Rifts: Europe and Asia. Tectonophysics 208, 55-75.

FIGURE CAPTIONS

Figure 1: (a) Simplified map of the main structural elements of the northern North Sea (modified from Riber et al., 2015). The red box indicate our study area, the white stippled line indicates the location of the regional cross-section X-X', while the thick green lines show the location of the major offshore and onshore Devonian intra-basement shear zones (from Fazlikhani et al., 2017). (b) Major and minor normal fault systems in the northwestern Utsira High and Heimdal Terrace, interpreted at the Base Sleipner Formation (time-structure map in background) structural level. (c) 2D regional geoseismic interpretation of the northern North Sea across the East Shetland Platform, South Viking Graben, HT-Heimdal Terrace, Utsira High, and Stord Basin. Abbreviations: GT, ST, LT, and UT = Gudrun, Sleipner, Lomre, and Uer terraces respectively; CS = Crawford Spur; BE = Beryl Embayment; USZ, HSZ, KSZ, SSZ, JSZ, ÅSZ, LSZ, BSZ, NSZ, PSZ, and BASZ = Utsira, Hardangerfjord, Karmøy, Stavanger, Jaeren, Åsta, Lomre, Brent, Ninian, Pobie, and Bergen Arc shear zones respectively; NSDZ = Nordfjord-Sogn Detachment Zone.

Figure 2: Generalized stratigraphic column within the study area, together with the major tectonic events that has taken place during the evolution of the present-day northern North Sea.

Figure 3: (a) SW-NE and (b) SSW-NNE seismic sections along the Utsira High showing some of the different patterns of intra-basement reflection (IBR) packages. (c) Uninterpreted and interpreted enlarged panel showing the amalgamated high amplitude reflections that characterises IBR1. (d) Uninterpreted and interpreted enlarged panel showing the low reflection amplitudes and splaying geometries that characterises IBR3. Note how IBR3 displaces the top Basement. (e) Uninterpreted and interpreted seismic section showing the low reflection

amplitude character and inclined geometry that characterises IBR2. Note that the top Basement truncates IBR2. See Fig. 4b for locations of the cross sections.

Figure 4: Uninterpreted and interpreted time slices at (a) -3992 ms TWT and (b) -5364 ms TWT from reflectivity intensity (RI) attribute, showing the enigmatic lateral and vertical geometry of intra-basement shear zones. The Utsira shear zone trend NE-SW, while the Heimdal shear zone exhibit a general E-W trend, but deflects approximately NNW in the northwestern part.

Figure 5: (a) Non-colinear rift fault network defined by two main structural domains; structural domain 1 (blue) and structural domain 2 (red) normal faults. The locations of T-x profiles and expansion index (EI) plots presented in Figs. 7 and 8 are indicated. (b) Rose plot of the orientation of structural domain 1 faults. (c) Rose plot of the orientation of structural domain 2 faults. The major trends of structural domain 1 and 2 are NE-SW and N-S respectively. (d) Map-view relationship between intra-basement shear zones and some major rift related normal faults.

Figure 6: (a) Uninterpreted and interpreted seismic section from the south of the study area, showing the vertical interaction between structural domain 1 faults and underlying shear zone. The Western Utsira High Fault (WUHF) detaches on the Utsira Shear Zone (‘merging fault’ interaction), while other nearby faults tip out above the Utsira Shear Zone (‘*kinematic* fault’ interaction). (b) Uninterpreted and interpreted seismic section from the north of the study area, showing the antithetic-synthetic and/or conjugate style faulting that characterises structural

domain 2. Some N-S-striking faults displaces the Heimdal Shear Zone ('cross-cutting fault' interaction). See Fig. 5a for locations of the cross sections.

Figure 7: (a) T-x profile of the NE-SW-striking WUHF showing the along-strike throw distribution at the Base Sleipner and Top Basement horizons, and the corresponding variance attribute map. Overall, the throw at the Base Sleipner horizon is greater than that of the Top Basement, suggesting that the fault nucleated within the sedimentary cover, then grew downwards into the Basement. (b) T-x profile of the N-S-striking HF1 showing the along-strike throw distribution at the Base Sleipner horizon, and the corresponding variance attribute map. (c) T-x profile of the N-S-striking HHF showing the along-strike throw distribution at the Base Sleipner horizon, and the corresponding variance attribute map.

Figure 8: Seismic sections with interpreted horizons and EI (expansion index) calculations of representative NE-SW- and N-S-striking rift faults, showing fault growth stratal geometries and timing of fault activity. (a) Geoseismic section (left) and EI plot (right) of the NE-SW-striking Western Utsira High Fault (WUHF). The growth strata exhibits two distinct geometries; tabular and wedge-shaped geometries. EI values from Top Basement – Top Dunlin Group are calculated from seismic, while EI values from Base Sleipner – Top Åsgard are calculated from Formation tops obtained from the Norwegian Petroleum Directorate FactPages (http://factpages.npd.no) for wells 25/8-9 (hangingwall) and 25/8-7 (footwall) (locations of the wells are shown in Fig. 1b and 5a). (b) Geoseismic section (left) and EI plot (right) of the N-S-striking Heimdal Fault (HF1). (c) Geoseismic section of the N-S-striking Fault H1.

Figure 9: (a-c) Simple conceptualized model of how pre-existing intra-basement shear zone influences the geometry and consequent development of non-colinear rift fault network in rift basins. (d) Cross-sectional tectono-sedimentary evolution model of the Western Utsira High Fault (WUHF) demonstrating the transition from non-rotational slip to rotation slip of hangingwall due to linkage and detachment on to the underlying pre-existing Utsira Shear Zone.

Figure 10: Schematic representation of the different paleostress configuration models proposed for the North Sea rift system during the Middle Jurassic – Early Cretaceous rift phase (RP2) in relation to the Permo-Triassic rift phase (RP1).

FIGURE 1

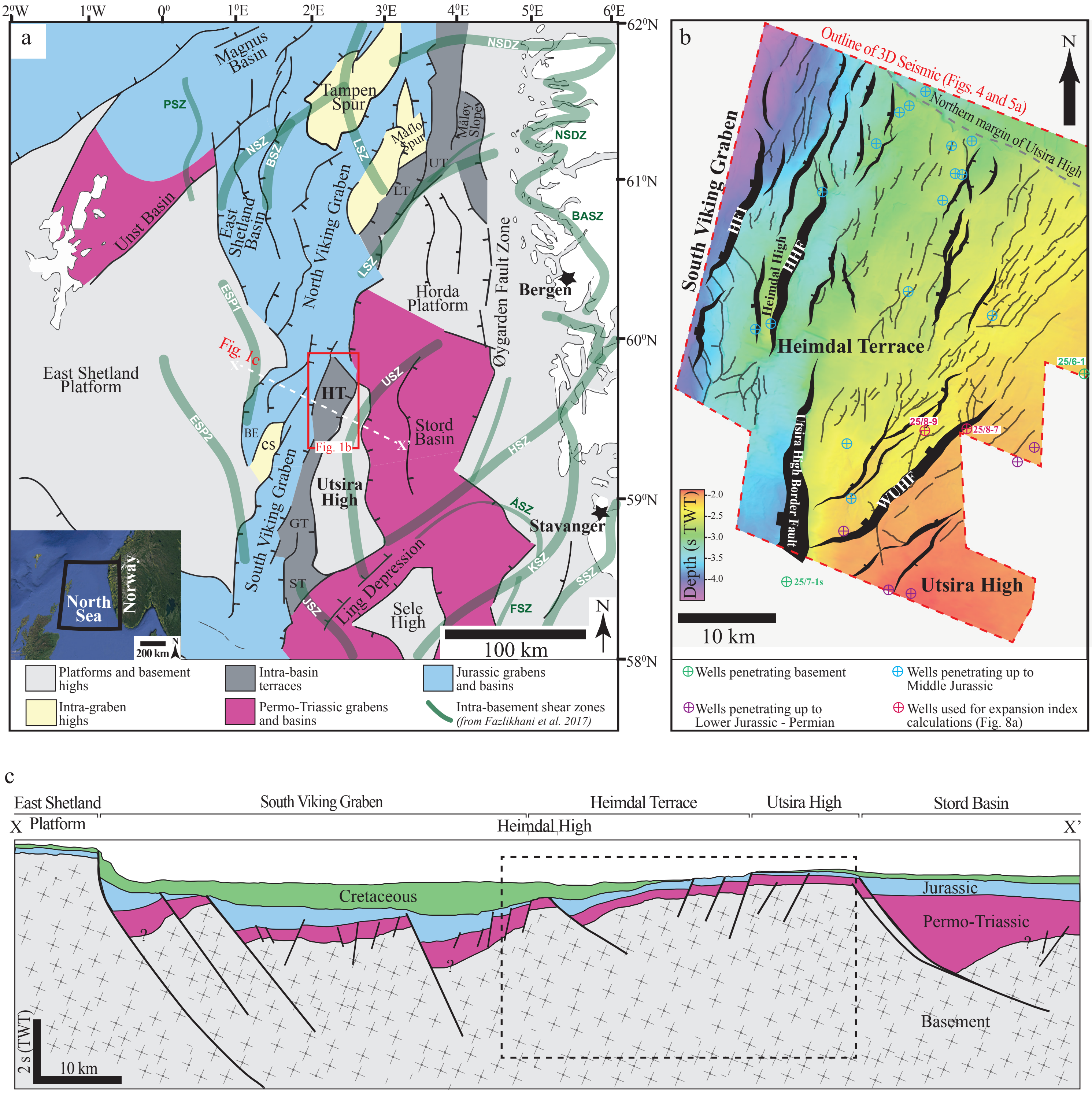
a
2⁰W
1⁰W
0⁰
1⁰E
2⁰E
3⁰E
4⁰E
5⁰E
6⁰E
62⁰N
61⁰N
60⁰N
59⁰N
58⁰N
Magnus Basin
Tampen Spur
Måløy Slope
Maflo Spur
NSDZ
PSZ
NSZ
BSZ
LSZ
UT
LT
Unst Basin
East Shetland Basin
North Viking Graben
BASZ
Horda Platform
Øygarden Fault Zone
Bergen
ESP1
Fig. 1c
X
HT
USZ
East Shetland Platform
Stord Basin
X'
ESP2
BE
CS
Fig. 1b
HSZ
Utsira High
ASZ
Stavanger
GT
South Viking Graben
KSZ
ST
Ling Depression
SSZ
JSZ
Sele High
FSZ
North Sea
Norway
200 km
N
100 km
Platforms and basement highs
Intra-basin terraces
Jurassic grabens and basins
Intra-graben highs
Permo-Triassic grabens and basins
Intra-basement shear zones (from Fazlikhani et al. 2017)
b
Outline of 3D Seismic (Figs. 4 and 5a)
Northern margin of Utsira High
South Viking Graben
HFI
Heimdal High
HHF
Heimdal Terrace
25/6-1
Utsira High Border Fault
25/8-9
25/8-7
WUHF
Depth (s TWT)
-2.0
-2.5
-3.0
-3.5
-4.0
25/7-1s
Utsira High
10 km
Wells penetrating basement
Wells penetrating up to Middle Jurassic
Wells penetrating up to Lower Jurassic - Permian
Wells used for expansion index calculations (Fig. 8a)
c
East Shetland Platform
South Viking Graben
Heimdal Terrace
Utsira High
Stord Basin
Heimdal High
X
X'
Cretaceous
Jurassic
Permo-Triassic
?
Basement
2 s (TWT)
10 km

FIGURE 2

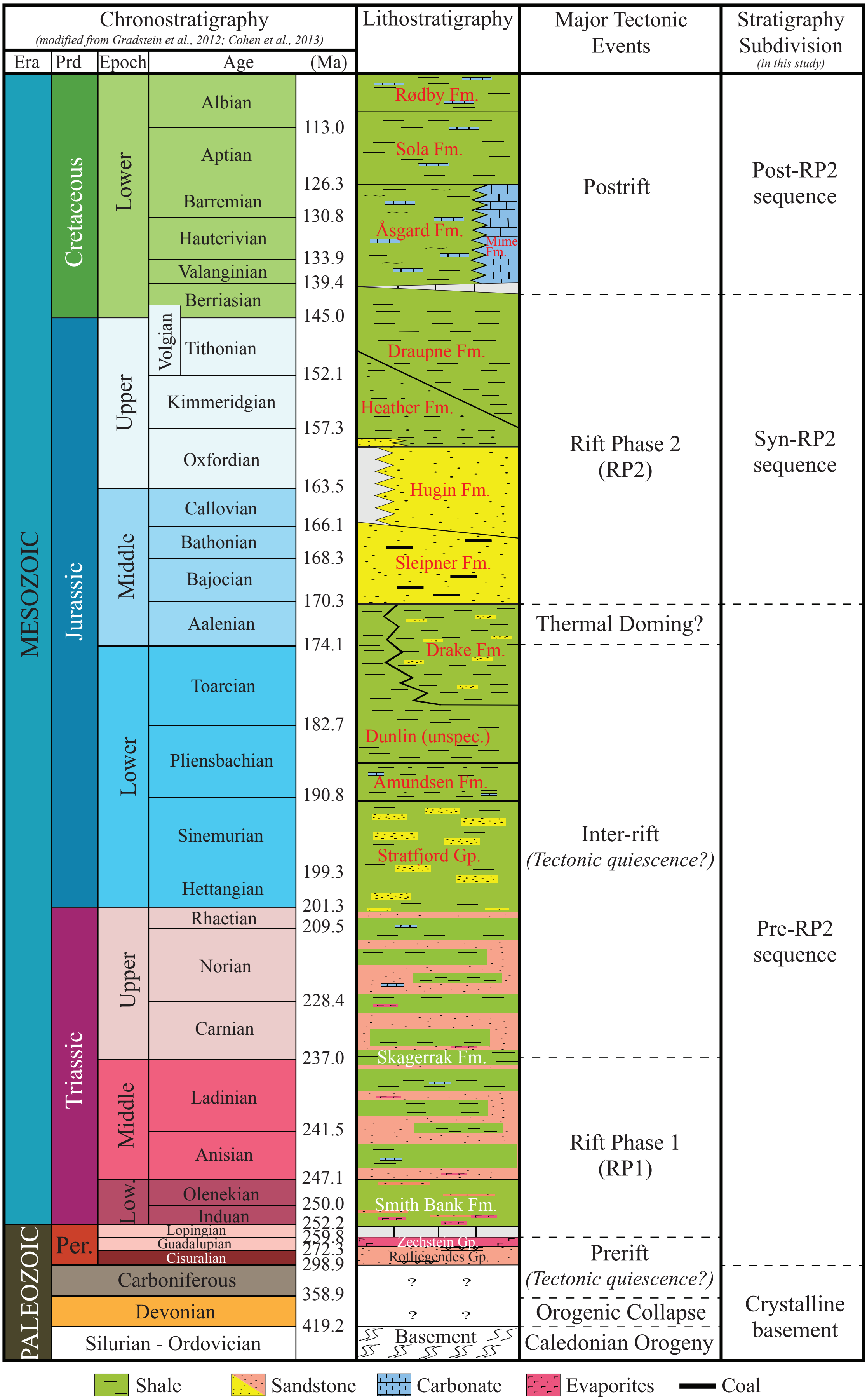
Chronostratigraphy
(modified from Gradstein et al., 2012; Cohen et al., 2013)
Era
Prd
Epoch
Age
(Ma)
Lithostratigraphy
Major Tectonic Events
Stratigraphy Subdivision
(in this study)
MESOZOIC
PALEOZOIC
Cretaceous
Jurassic
Triassic
Per.
Lower
Upper
Middle
Low.
Volgian
Albian
Aptian
Barremian
Hauterivian
Valanginian
Berriasian
Tithonian
Kimmeridgian
Oxfordian
Callovian
Bathonian
Bajocian
Aalenian
Toarcian
Pliensbachian
Sinemurian
Hettangian
Rhaetian
Norian
Carnian
Ladinian
Anisian
Olenekian
Induan
Lopingian
Guadalupian
Cisuralian
Carboniferous
Devonian
Silurian - Ordovician
113.0
126.3
130.8
133.9
139.4
145.0
152.1
157.3
163.5
166.1
168.3
170.3
174.1
182.7
190.8
199.3
201.3
209.5
228.4
237.0
241.5
247.1
250.0
252.2
259.8
272.3
298.9
358.9
419.2
Rødby Fm.
Sola Fm.
Åsgard Fm.
Mime Fm
Draupne Fm.
Heather Fm.
Hugin Fm.
Sleipner Fm.
Drake Fm.
Dunlin (unspec.)
Amundsen Fm.
Stratfjord Gp.
Skagerrak Fm.
Smith Bank Fm.
Zechstein Gp.
Rotliegendes Gp.
Basement
Postrift
Rift Phase 2
(RP2)
Thermal Doming?
Inter-rift
(Tectonic quiescence?)
Rift Phase 1
(RP1)
Prerift
(Tectonic quiescence?)
Orogenic Collapse
Caledonian Orogeny
Post-RP2 sequence
Syn-RP2 sequence
Pre-RP2 sequence
Crystalline basement
Shale
Sandstone
Carbonate
Evaporites
Coal

FIGURE 3

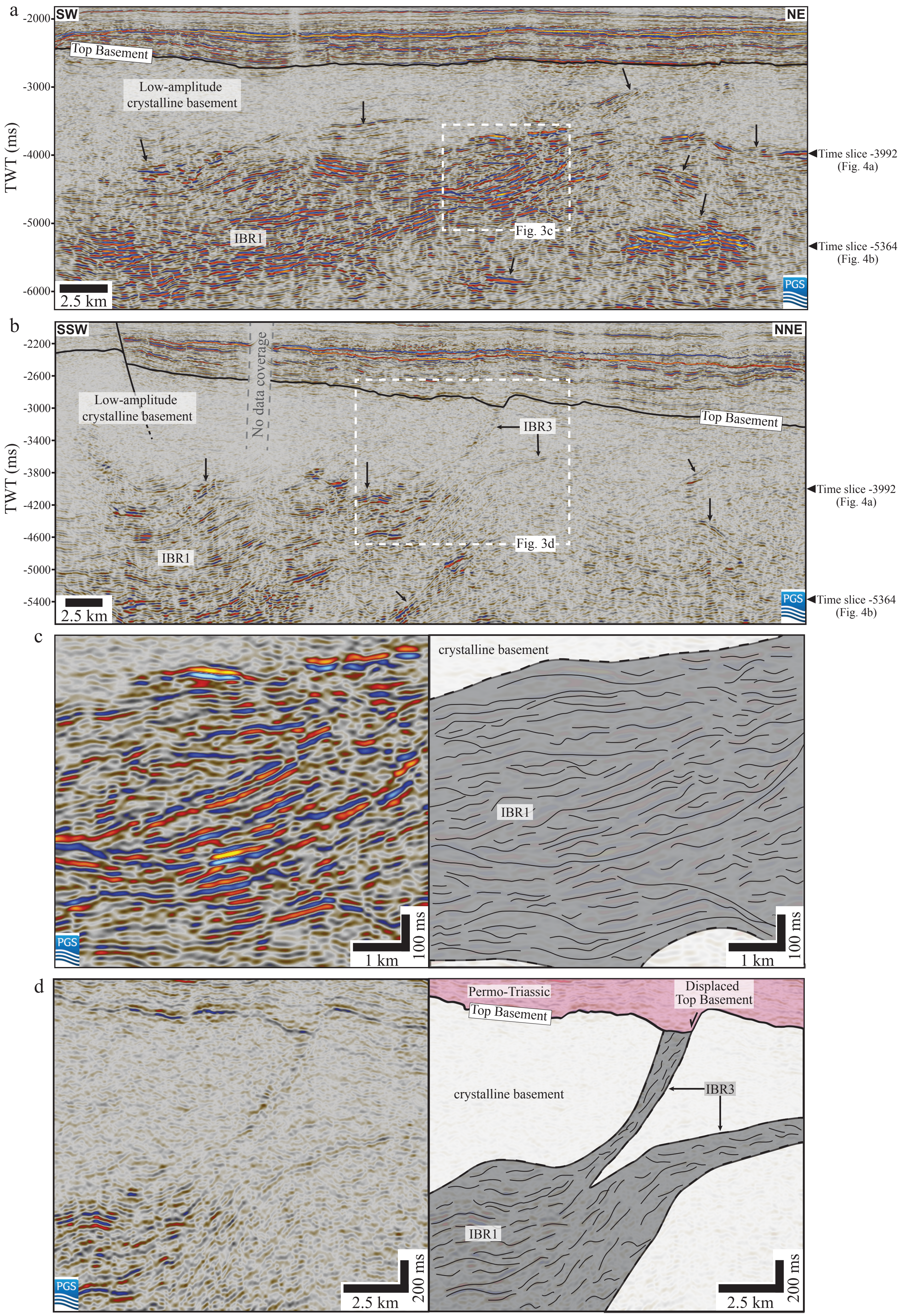
a
SW
NE
Top Basement
Low-amplitude crystalline basement
IBR1
Fig. 3c
TWT (ms)
-2000
-3000
-4000
-5000
-6000
2.5 km
Time slice -3992 (Fig. 4a)
Time slice -5364 (Fig. 4b)
PGS
b
SSW
NNE
No data coverage
Low-amplitude crystalline basement
IBR3
Top Basement
IBR1
Fig. 3d
-2200
-2600
-3000
-3400
-3800
-4200
-4600
-5000
-5400
2.5 km
c
crystalline basement
IBR1
1 km
100 ms
d
Permo-Triassic
Top Basement
Displaced Top Basement
crystalline basement
IBR3
IBR1
2.5 km
200 ms

FIGURE 3 Cont.

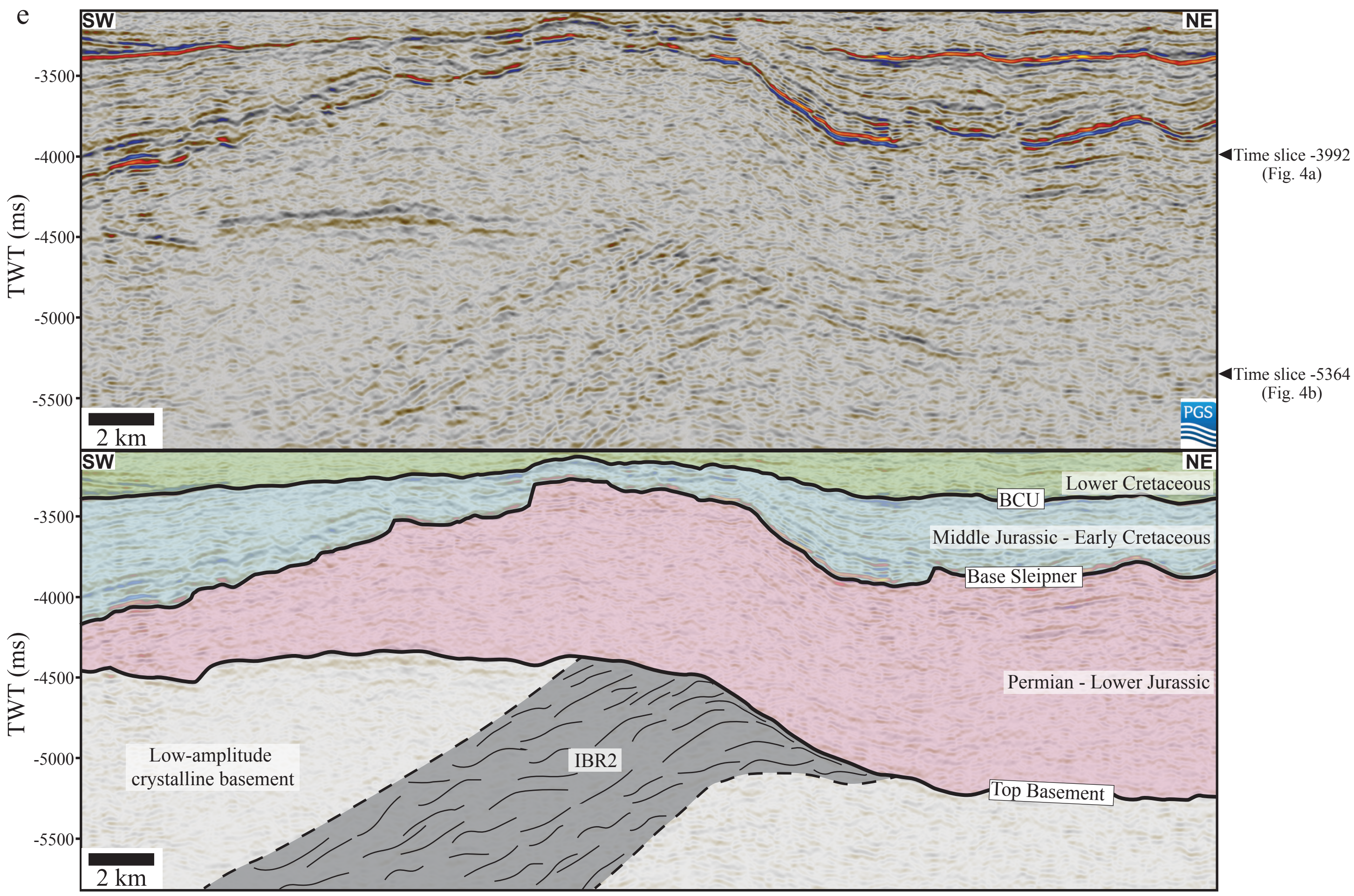

FIGURE 4

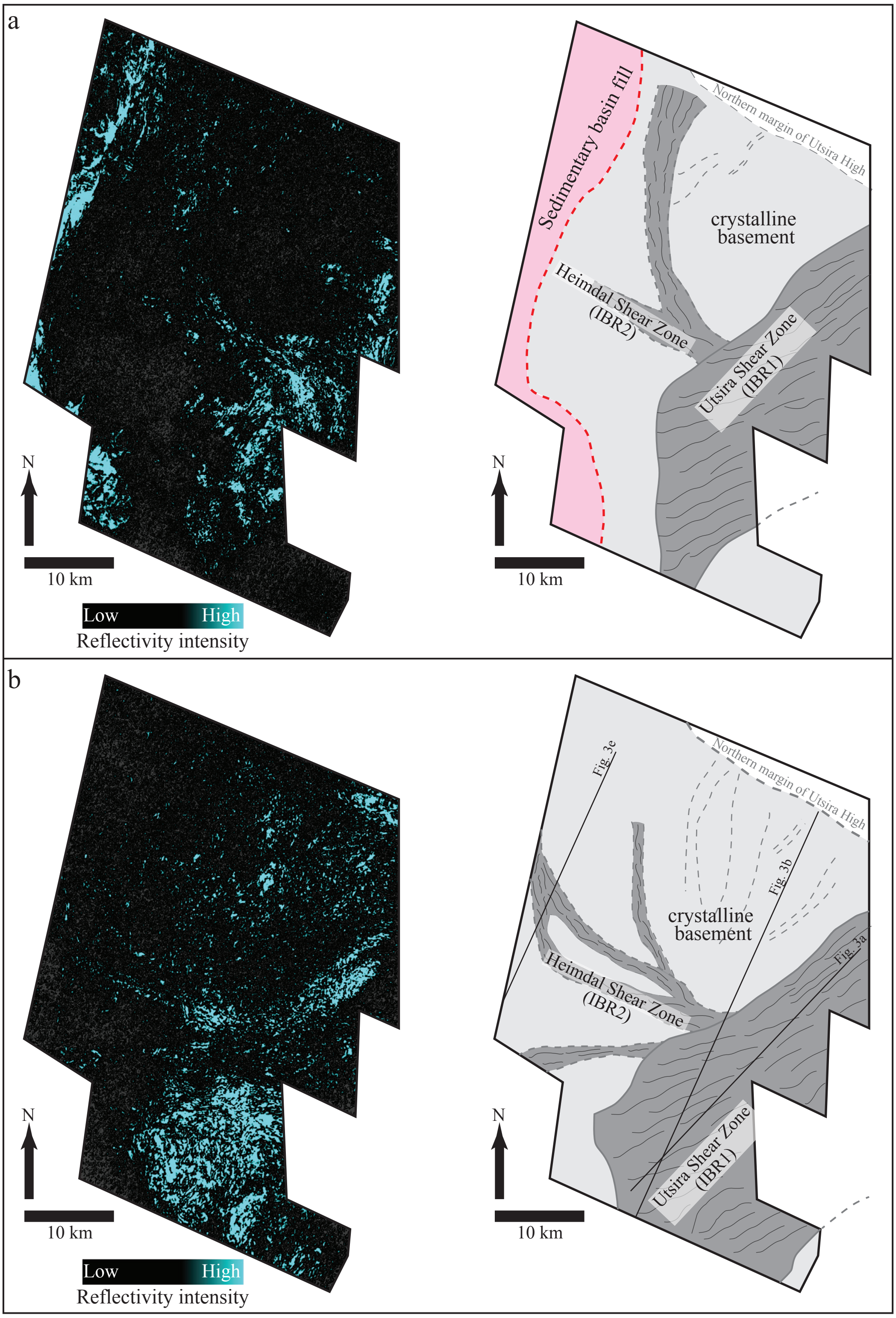

a
N
10 km
Low
High
Reflectivity intensity
Sedimentary basin fill
Northern margin of Utsira High
crystalline basement
Heimdal Shear Zone (IBR2)
Utsira Shear Zone (IBR1)
b
Fig. 3e
Fig. 3b
Fig. 3a

FIGURE 5

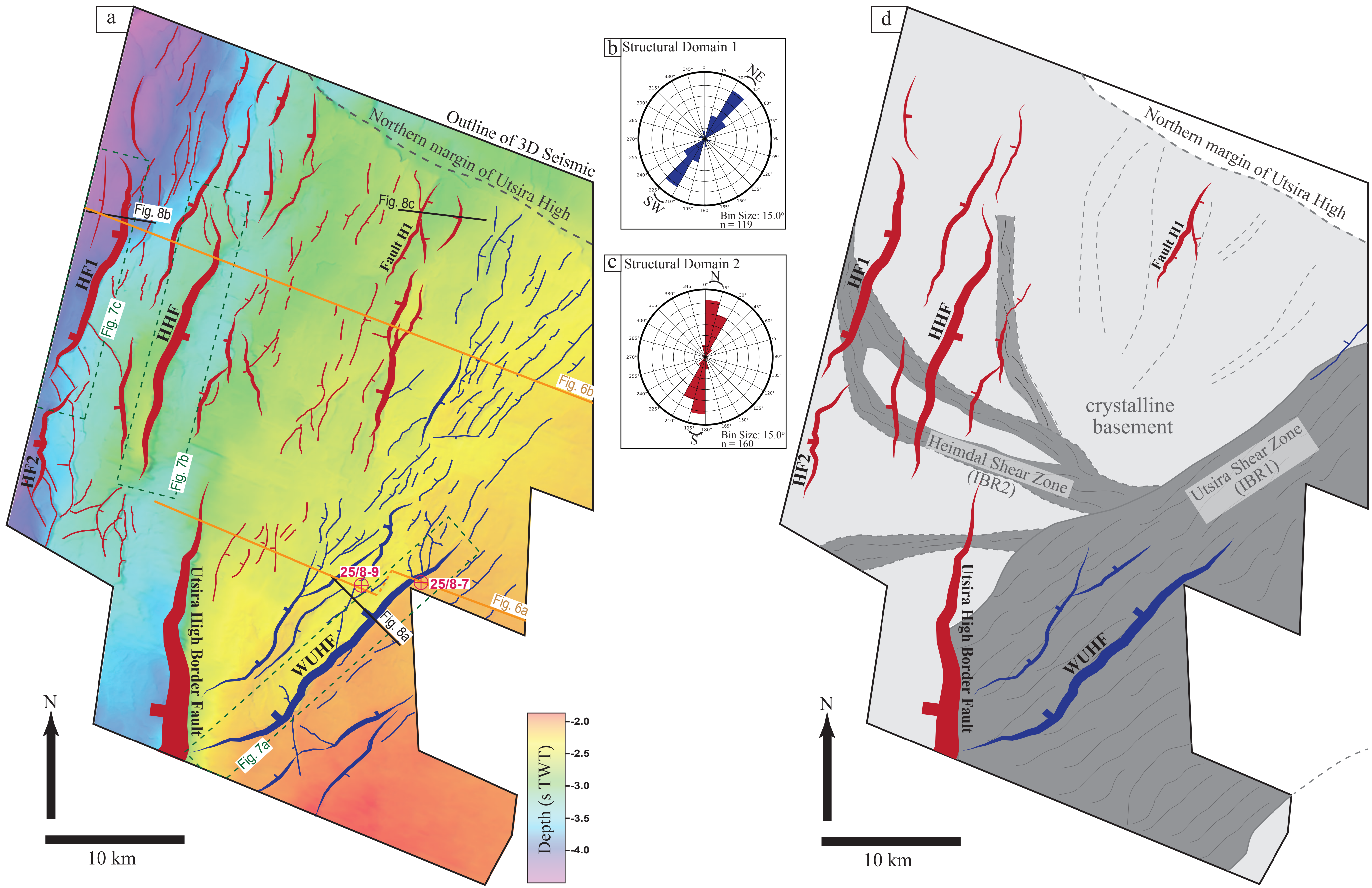
a
Outline of 3D Seismic
Northern margin of Utsira High
Fig. 8b
Fig. 8c
Fault H1
HF1
HHF
HF2
Fig. 7c
Fig. 7b
Fig. 6b
Fig. 6a
Fig. 8a
Fig. 7a
25/8-9
25/8-7
WUHF
Utsira High Border Fault
Depth (s TWT)
-2.0
-2.5
-3.0
-3.5
-4.0
N
10 km
b
Structural Domain 1
NE
SW
Bin Size: 15.0º
n = 119
c
Structural Domain 2
N
S
Bin Size: 15.0º
n = 160
d
Northern margin of Utsira High
Fault H1
HF1
HHF
HF2
crystalline
basement
Heimdal Shear Zone
(IBR2)
Utsira Shear Zone
(IBR1)
Utsira High Border Fault
WUHF
N
10 km

FIGURE 6

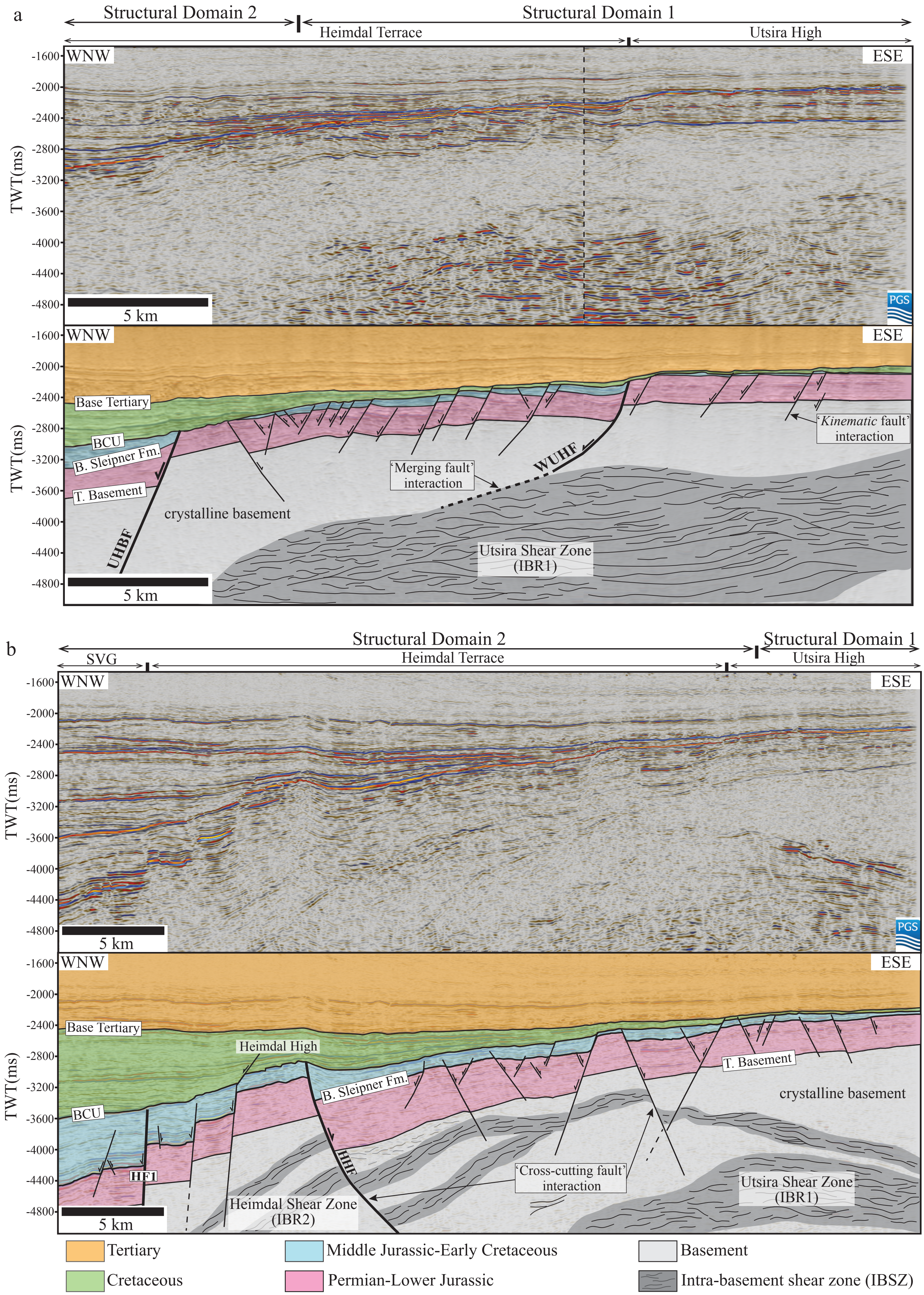
a
Structural Domain 2
Structural Domain 1
Heimdal Terrace
Utsira High
WNW
ESE
TWT(ms)
-1600
-2000
-2400
-2800
-3200
-3600
-4000
-4400
-4800
5 km
PGS
Base Tertiary
BCU
B. Sleipner Fm.
T. Basement
crystalline basement
UHBF
'Merging fault' interaction
WUHF
'Kinematic fault' interaction
Utsira Shear Zone (IBR1)
b
Structural Domain 2
Structural Domain 1
SVG
Heimdal Terrace
Utsira High
Heimdal High
B. Sleipner Fm.
T. Basement
crystalline basement
HF1
HHF
Heimdal Shear Zone (IBR2)
'Cross-cutting fault' interaction
Utsira Shear Zone (IBR1)
Tertiary
Cretaceous
Middle Jurassic-Early Cretaceous
Permian-Lower Jurassic
Basement
Intra-basement shear zone (IBSZ)

FIGURE 7

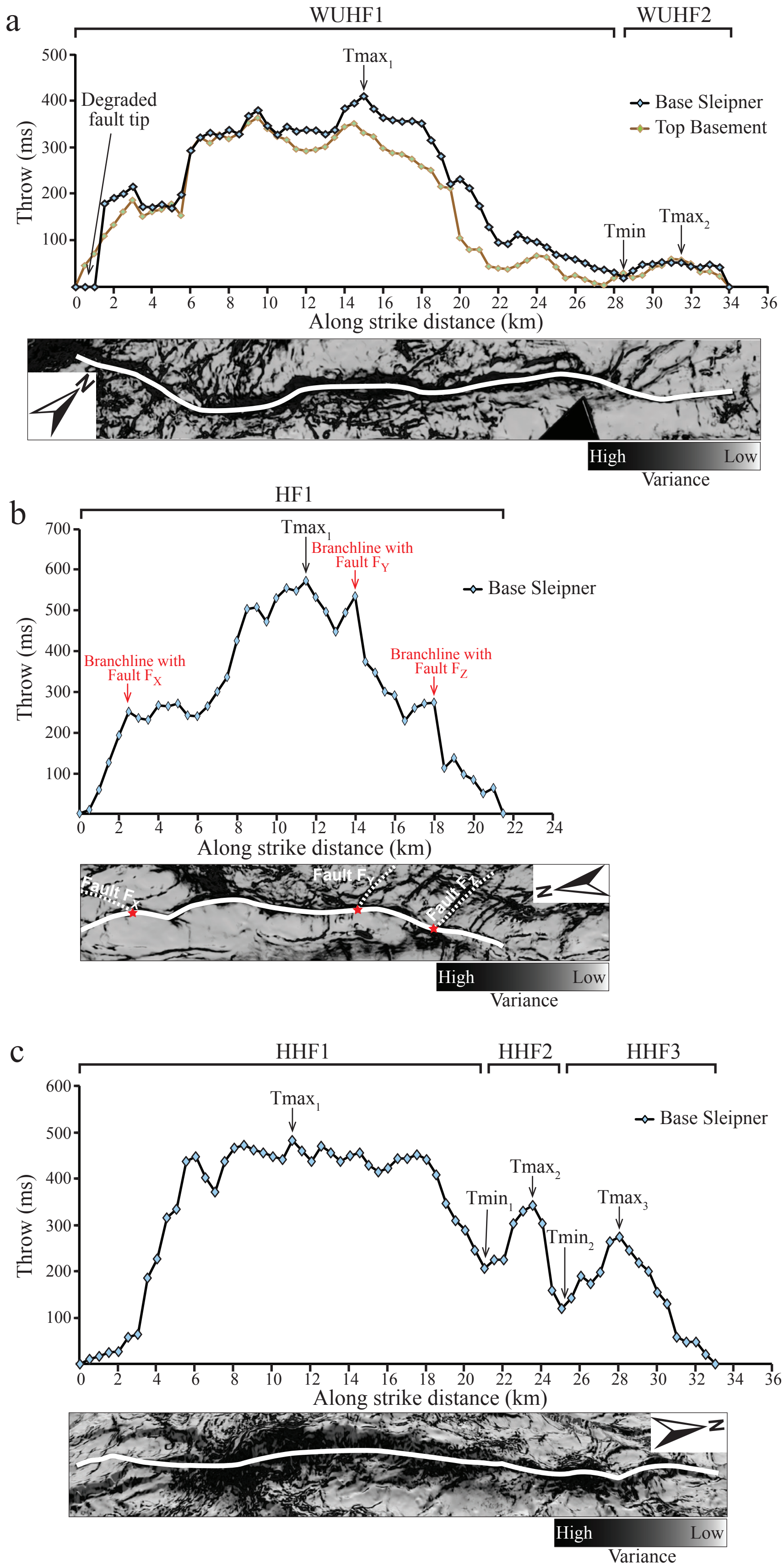
a
WUHF1
WUHF2
Throw (ms)
500
400
300
200
100
Degraded fault tip
Tmax$_1$
Base Sleipner
Top Basement
Tmin
Tmax$_2$
0 2 4 6 8 10 12 14 16 18 20 22 24 26 28 30 32 34 36
Along strike distance (km)
N
High
Low
Variance
b
HF1
Throw (ms)
700
600
500
400
300
200
100
Tmax$_1$
Branchline with Fault F_Y
Base Sleipner
Branchline with Fault F_X
Branchline with Fault F_Z
0 2 4 6 8 10 12 14 16 18 20 22 24
Along strike distance (km)
Fault F_X
Fault F_Y
Fault F_Z
N
High
Low
Variance
c
HHF1
HHF2
HHF3
Throw (ms)
600
500
400
300
200
100
Tmax$_1$
Base Sleipner
Tmax$_2$
Tmin$_1$
Tmin$_2$
Tmax$_3$
0 2 4 6 8 10 12 14 16 18 20 22 24 26 28 30 32 34 36
Along strike distance (km)
N
High
Low
Variance

FIGURE 8

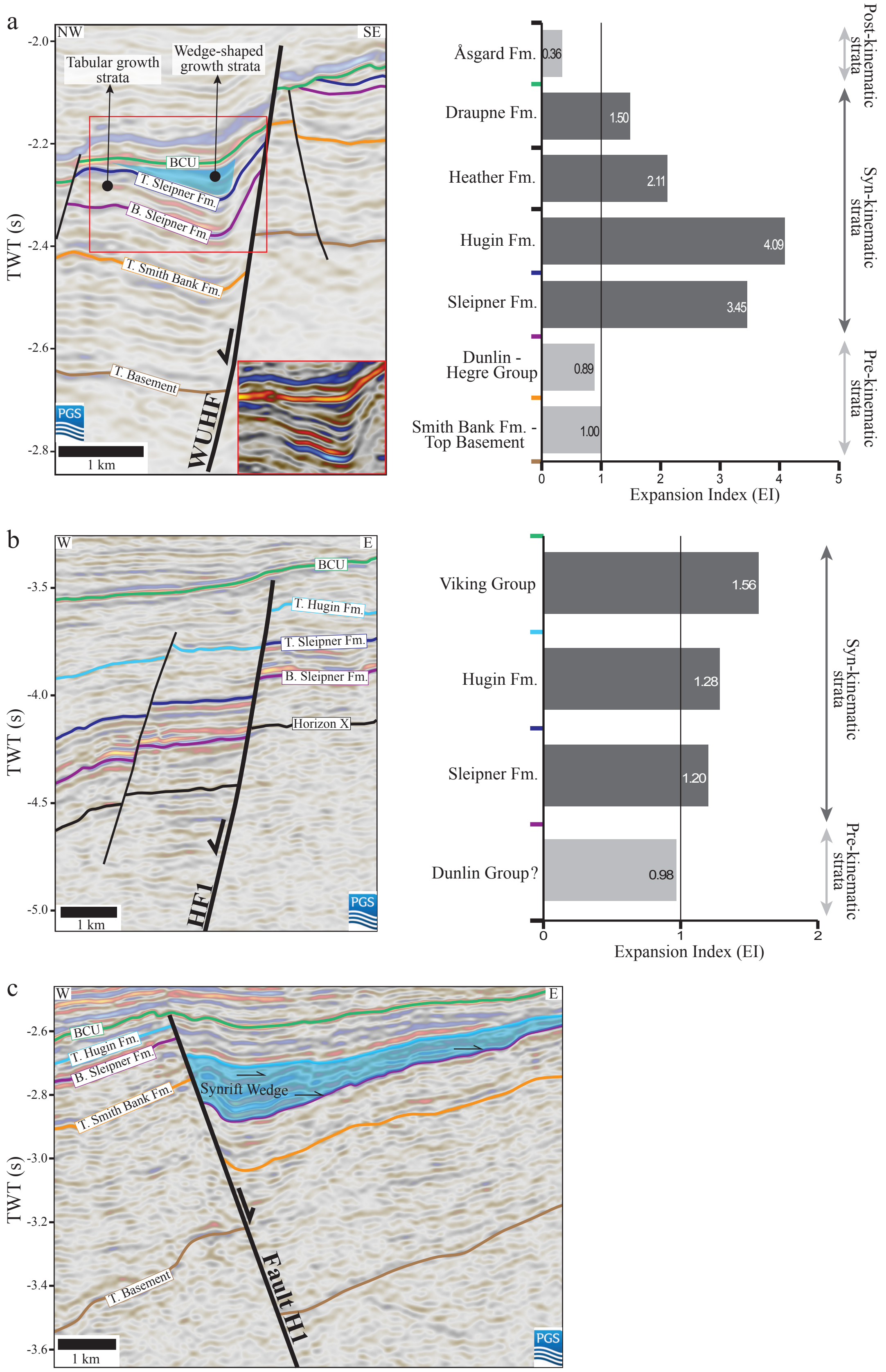
a
NW
SE
Tabular growth strata
Wedge-shaped growth strata
BCU
T. Sleipner Fm.
B. Sleipner Fm.
T. Smith Bank Fm.
T. Basement
WUHF
PGS
1 km
TWT (s)
-2.0
-2.2
-2.4
-2.6
-2.8
Åsgard Fm.
0.36
Draupne Fm.
1.50
Heather Fm.
2.11
Hugin Fm.
4.09
Sleipner Fm.
3.45
Dunlin - Hegre Group
0.89
Smith Bank Fm. - Top Basement
1.00
Expansion Index (EI)
0
1
2
3
4
5
Post-kinematic strata
Syn-kinematic strata
Pre-kinematic strata
b
W
E
BCU
T. Hugin Fm.
T. Sleipner Fm.
B. Sleipner Fm.
Horizon X
HF1
PGS
1 km
TWT (s)
-3.5
-4.0
-4.5
-5.0
Viking Group
1.56
Hugin Fm.
1.28
Sleipner Fm.
1.20
Dunlin Group?
0.98
Expansion Index (EI)
0
1
2
Syn-kinematic strata
Pre-kinematic strata
c
W
E
BCU
T. Hugin Fm.
B. Sleipner Fm.
T. Smith Bank Fm.
Synrift Wedge
T. Basement
Fault H1
PGS
1 km
TWT (s)
-2.6
-2.8
-3.0
-3.2
-3.4
-3.6

FIGURE 9

a

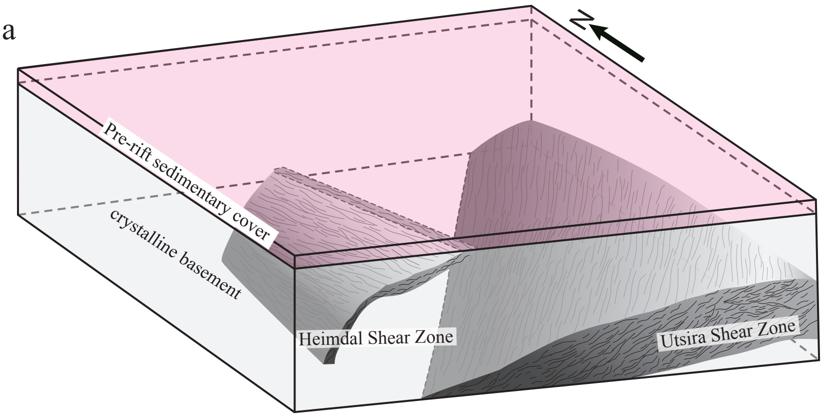

b

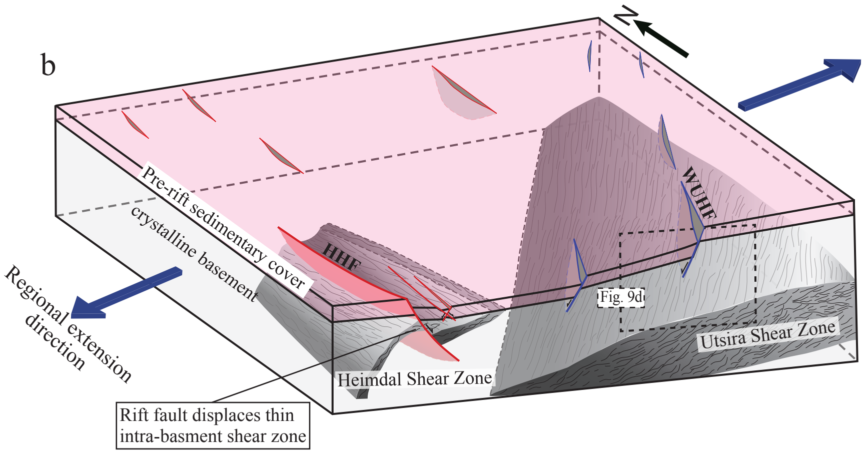

c

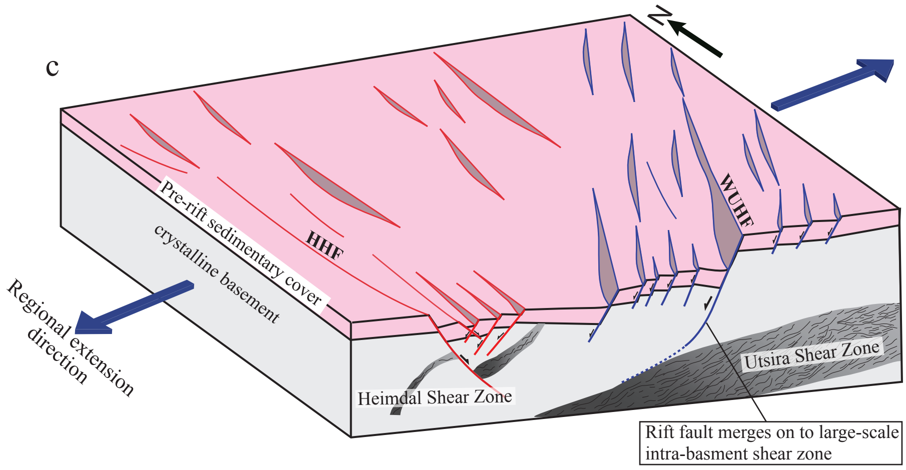

(a) Pre-extension configuration of the sedimentary cover and the underlying crystalline basement with multi-scale pre-existing shear zones.

(b) Early stage: Simultaneous formation of few isolated NE-SW- (blue) and N-S-striking (red) faults. Localised pertubation of the regional stress field due to the presence of underlying reactivated shear zone control the development of NE-SW-striking faults, while N-S-striking faults form in response to unperturbed regional stress field.

(c) Late stage: Interaction and linkage of early stage faults and nucleation of new faults.   .

d

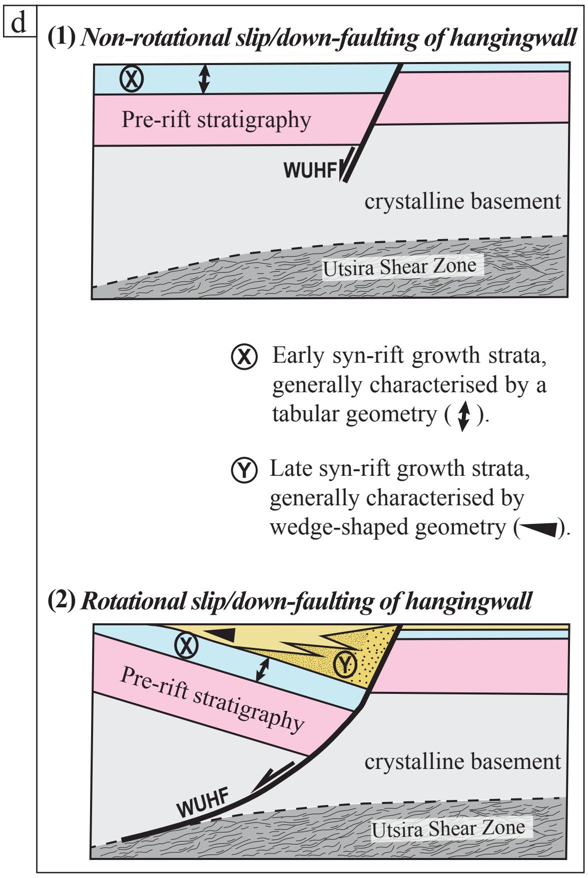

FIGURE 10

Model	Palaeo-stress Configuration (RP1 = Rift Phase 1; RP2 = Rift Phase 2)	Characteristics
1. Non-coaxial (different stress orientation) e.g., Færseth (1996); Færseth et al., (1997)	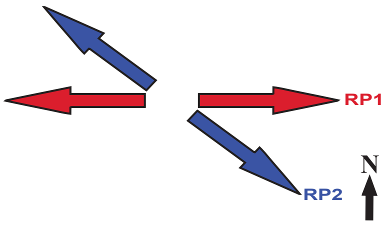	Major fault trends: N-S (RP1) and NE-SW (RP2) Controls on fault trend: Change in regional extension direction. Relative age of faults: N-S-striking faults are older than NE-SW-striking faults. Fault distribution: No localization of any fault trend is expected.
2a. Rotational (single phase rotation of RP2 extension direction) e.g., Doré and Gage (1987); Doré et al., (1997)	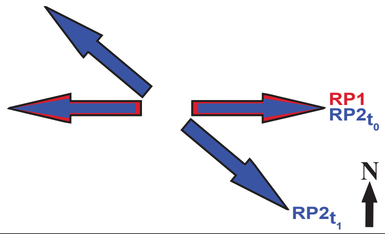	Major fault trends: N-S (RP1 and RP2) and NE-SW (RP2) Controls on fault trend: Rotation of RP2 extension direction. Relative age of faults: N-S-striking faults of RP1 are the oldest. N-S-striking faults of RP2 are older than NE-SW-striking (RP2) faults, depending on the timing of regional stress rotation. Fault distribution: No localization of any fault trend is expected.
2b. Rotational (two phase rotation of RP2 extension direction) e.g., Davies et al. (2001)	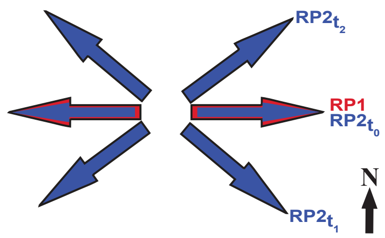	Major fault trends: N-S (RP1 and RP2), NE-SW and NW-SE (RP2) Controls on fault trend: Rotation of RP2 extension direction. Relative age of faults: N-S-striking faults of RP1 are the oldest. With respect to RP2, N-S-striking faults are the oldest, while NW-SE-striking are the youngest. Fault distribution: No localization of any fault trend is expected.
3. Coaxial (Constant stress orientation) e.g., Bartholomew et al., (1993); Reeve et al., (2015)	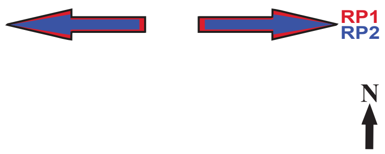	Major fault trends: N-S (RP1 and RP2) and NE-SW (RP2) Controls on fault trend: Local stress perturbation or re-orientation induced by underlying pre-existing weak zones. Relative age of faults: N-S- and NE-SW striking faults of RP2 nucleates simultaneously. Fault distribution: Localization of NE-SW-striking faults in the vicinity of the underlying pre-existing weak zone.